Cancer Biol Med 2025. doi: 10.20892/j.issn.2095-3941.2024.0596

ORIGINAL ARTICLE

Mitochondrial transplantation sensitizes chemotherapy to inhibit tumor development by enhancing anti-tumor immunity

Shumeng Lin[1,2*], Liuliu Yuan[1,2*], Xiao Chen[1,2,3*], Shiyin Chen[1,2*], Mengling Wei[1,2], Bingjie Hao[1,2], Tiansheng Zheng[1,2], Lihong Fan[1,2,4]

[1]Institute of Energy Metabolism and Health, Shanghai Tenth People's Hospital, Tongji University School of Medicine, Shanghai 200072, China; [2]Department of Respiratory Medicine, Shanghai Tenth People's Hospital, Tongji University School of Medicine, Shanghai 200072, China; [3]Department of Oncology, School of Medicine, Nantong University, Nantong 226007, China; [4]Department of Pulmonology, Sixth People's Hospital Affiliated to Shanghai Jiao Tong University, Shanghai 201306, China

ABSTRACT

Objective: Lung cancer is the leading cause of cancer-related deaths worldwide. Chemotherapy is associated with side effects, such as damage to myeloid cells and a reduction in the number of immune cells in patients. In addition, tumor cells hijack the mitochondria of immune cells through tunnel nanotubes, thereby weakening immune ability.

Methods: In this study the effects of direct mitochondria transplantation on cancer cell proliferation and chemotherapeutic sensitivity were determined, as well as anti-tumor immunity in *in vitro* and *in vivo* lung cancer models.

Results: A combination of mitochondrial transplantation and cisplatin chemotherapy was shown for the first time to significantly improve immune infiltration of advanced non-small cell lung cancer (NSCLC) and overcome the shortcomings of cisplatin chemotherapy, including damage to myeloid cells and a reduction in the number of immune cells.

Conclusions: The findings of the current study provide valuable recommendations for enhancing immune infiltration and augmenting anti-tumor efficacy during chemotherapy in advanced NSCLC. In addition, the findings support "mitochondrial transfer" as a novel paradigm in tumor treatment.

KEYWORDS Lung cancer; mitochondria transplantation; anti-tumor immunity; chemotherapy; cisplatin

Introduction

Lung cancer is the most prevalent malignant tumor and has the highest mortality rate worldwide. Approximately 2.5 million individuals were newly diagnosed with lung cancer in 2022, constituting 12.4% of all cancer cases worldwide. There were 1.82 million lung cancer-related deaths in 2022, making up approximately 18.7% of all cancer mortalities[1]. Non-small cell lung cancer (NSCLC) represents 85% of the different histopathologic forms of lung cancer[2]. Chemotherapy is the most frequently used first-line therapy for advanced NSCLC but the efficacy of chemotherapy is decreased by drug resistance[3]. In addition, myeloid cell destruction and a reduction in the number of immune cells are among the several side effects frequently accompanying chemotherapy[4].

Tumor immunotherapy has advanced dramatically in the past few decades. Tumor immunotherapy stimulates or modulates the immune system to improve immune responses within the tumor microenvironment to inhibit or eliminate tumor cells[5,6]. Tumor immunotherapy has evolved into the fourth tumor treatment paradigm, after cancer surgery, chemotherapy, and radiation therapy. Tumor immunotherapy is based on a combination of several methodologies with cutting-edge biological technology[7]. Furthermore, different and highly adaptive T cell receptors can specifically counter chemotherapy resistance. Hence, it is essential to augment the immune response against malignancies for the duration of chemotherapy in patients with NSCLC[8].

*These authors contributed equally to this work.
Correspondence to: Liuliu Yuan and Lihong Fan
E-mail: m18051981957@163.com and fanlih@aliyun.com
ORCID ID: https://orcid.org/0009-0001-5291-6622 and https://orcid.org/0009-0005-9088-8772
Received December 17, 2024; accepted April 25, 2025;
published online June 19, 2025.
Available at www.cancerbiomed.org
©2025 The Authors. Creative Commons Attribution-NonCommercial 4.0 International License

Mitochondria supply energy for cell survival and are among the most critical organelles in eukaryotic cells. Defective mitochondria can harm cells and organs. Moreover, multiple illnesses, including cancers, have been associated with mitochondrial abnormalities[9]. One of the primary distinctions between malignant and normal cells is that tumor cells undergo metabolic reprogramming. In addition, tumor mitochondria contribute to metabolic reprogramming. Malignant tumor cells frequently alter the quantity, shape, and function of mitochondria to promote rapid proliferation in an acidic and hypoxic environment. Therefore, mitochondrial transplantation has been implemented in tumor therapy[10,11]. It has been reported that a significant number of oxygen radicals are generated immediately following mitochondrial transplantation into cancerous tissue under hypoxic and acidic conditions, which results in cell death. This effect can eliminate tumor cells and repair destroyed tissue function. Furthermore, it has been demonstrated that tumor cells use tunnel nanotubes (TNTs) to hijack the mitochondria of immune cells, which impairs the ability of immune cells to fight[12]. TNT-mediated mitochondrial transfer from bone marrow stromal cells (BMSCs) can boost CD8+ T cell bioenergetic capabilities and anti-tumor efficacy[13]. Inhibiting nanotube synthesis interrupts tumor cells from hijacking mitochondria or promoting intercellular mitochondrial transfer, thus enhancing mitochondrial function of tumor-infiltrating lymphoid cells and improving anti-cancer effectiveness.

We hypothesize that immune cell immunity can be strengthened by introducing healthy mitochondria into immune cells in tumor-infiltrating regions. No studies have demonstrated that mitochondrial transplantation can boost immune cell infiltration. Indeed, we have demonstrated that a combination of mitochondrial transplantation and cisplatin treatment greatly improves immune cell infiltration of advanced NSCLC, thereby overcoming the limitations of cisplatin chemotherapy, such as myeloid cell destruction and reduced immune cell number. This study has provided a new strategy for cancer immunotherapy by boosting anti-tumor immunity through a combination of mitochondrial transplantation and cisplatin treatment.

Materials and methods

Cell culture and reagents

Human cardiac cells (AC16) and mouse lung cancer cells [Lewis lung carcinoma (LLC)] were provided by the Chinese Academy of Sciences Cell Bank (Shanghai, China). The cells were cultivated in DMEM medium with 5% fetal bovine serum added as a supplement. The cells were kept in an incubator at a maintained temperature of 37°C and 5% CO_2. The medium was changed every 2 d. All cells were utilized within 10 passages or resuscitated within 1 month.

Isolation and transplantation of mitochondria

AC16 cells were extracted by differential centrifugation using a Cell Mitochondria Isolation kit (catalog # C3601; Beyotime, Shanghai, China) according to the manufacturer's instructions. AC16 cells were digested using trypsin and counted at 70% confluence. Cells were treated with mitochondria isolation reagent to isolate mitochondria, then homogenized approximately 30 times with a glass homogenizer until one-half of the cells were stained with trypan blue and centrifuged (1,000 × *g* for 10 min) to remove nuclei and debris. The mitochondria sedimented following centrifugation of the supernatant for 10 min at 12,000 × *g*, while the supernatant contained organelles with greater sedimentation coefficients, such as ribosomes. Isolation of mitochondria was performed within 30 min in a sterile setting at 4°C. The sediment was aliquoted and dissolved in PBS after the second centrifugation. The total quantity of mitochondria was calculated based on the quantity of AC16 cells used. The Multisizer 4e Coulter Counter (Beckman-Coulter, Brea, CA, USA) was used to measure the number of mitochondria and hemocytometry was used to confirm the results. The mitochondria were subsequently resuspended with medium to the indicated concentrations and added to the cells. The mitochondria were resuspended with normal saline solution to the indicated concentrations for *in vivo* use. Mitochondrial transplantation was performed locally and systemically via intra-tumoral (50 μL) and tail vein injection (200 μL), respectively; the total number of transplanted mitochondria was 1×10^7 per animal.

Mitochondrial uptake and internalization

LLC cells were seeded on a flat-bottomed 6-well plate and allowed to attach for 24 h at 37°C in a 5% CO_2 environment. Cell cultures were carried out exactly as above. MitoTracker® Green FM (Yeasen, Shanghai, China) is a cell-permeable structural derivative of carbocyanine containing a weakly sulfhydryl-reactive chloromethyl functional group that labels mitochondria. FM is a fluoromethyl ester group (cell membrane permeable form, hydrolyzed, and retained in mitochondria).

The corresponding concentrations of MitoTracker® Green FM was used to label endogenous mitochondria in LLC cells to distinguish the endogenous mitochondria from transplanted exogenous mitochondria. Lentiviral particles used to label the mitochondria in 293T cells were purchased from Hanbio Tech (Shanghai, China). The construct was designated pCMV-Mito-DsRed-puro and contained the mitochondrial targeting sequence of human cytochrome c oxidase subunit VIII and the codon-optimized red fluorescent protein DsRed gene. This transduction enabled the 293T cells to stably express the Mito-DsRed fusion protein. Mitochondria were isolated from 293T cells, avoiding false-positives caused by dye off target. LLC cells were co-cultured with DsRed-labeled exogenous mitochondria to determine whether LLC cells could take up exogenous mitochondria. Finally, LLC cells nuclei were stained with Hoechst 33342 (0.5 μg/mL; Sigma, San Francisco, CA, USA) for 30 min at 37°C.

Mitochondria viability

Isolated mitochondria viability was assessed using fluorescence microscopy and fluorescence-activated cell sorting (FACs). The lentivirus (pCMV-Mito-DsRed-puro; Hanbio Tech) was transduced into 293T cells. Mitochondria were tagged with DsRed, isolated, and photographed under a fluorescence microscope. Chloromethyl-X-rosamine (CMXRos) is a cell-permeable X-rosamine derivative. The aggregation of Mito-Tracker Red CMXRos (Yeasen) within mitochondria is dependent on the membrane potential of the mitochondria, thus enabling specific labeling of biologically active mitochondria. MitoTracker® Red CMXRos-stained mitochondria from AC16 cells were examined using a BD LSRFortessa flow cytometer (BD Bioscience, NJ, USA).

The function of isolated mitochondria was determined using the ATPlite luminescent ATP detection system (Molecule Devices, Shanghai, China). An ATP standard was used as a positive control and PBS solution served as a negative control. ATP values were determined for 1×10^7 mitochondria. Luminescence was measured using a SpectraMax iD5 multifunction microplate reader (Molecule Devices, Shanghai, China).

Cell proliferation test in vitro and in vivo

An equal number of LLC cells were seeded in 96-well plates to perform cell growth tests *in vitro*. CCK-8 reagent (Beyotime Biotechnology, Shanghai, China) was applied according to the manufacturer's instructions and absorbance at 450 nm was measured to determine the cell proliferation rate. EdU assays were carried out using an EdU Cell Proliferation Assay kit (ST067; Beyotime) according to the manufacturer's instructions. Male C57BL/6 mice (n = 5; Charles River Laboratories, Shanghai, China) were given a subcutaneous injection of 1×10^6 LLC cells into the right dorsal side for the purpose of an *in vivo* tumor cell growth assay. The following formula was used to calculate the tumor volume: (length*width*width)/2. The data were weighted after 25 d. The present study was approved (Approval No. SHDSYY-2024-7001) by the Institutional Animal Care and Use Committee of Shanghai Tenth People's Hospital Affiliated to Tongji University School of Medicine (Shanghai, China).

Immunohistochemical (IHC)

Fresh tumors were preserved with 10% neutral buffered formalin overnight before embedding in paraffin. The specimens were cut into 5-μm pieces, dried overnight at 60°C, and stained with hematoxylin and eosin (H&E) and antibodies. K-viewer software (Ningbo Konfoong Bioinformation Tech Co., Ningbo, China) was utilized to verify each IHC staining area after being photographed using panoramic MIDI (Thermofisher, MA, USA).

Western blotting

Following drug treatment the cells were rinsed 3 times with PBS before 100 μL of RIPA Lysis Buffer (Yeasen, Shanghai, China) was added to each 6-well plate. Centrifugation was used to extract the entire cell lysate of LLC cells at 4°C and 12,000 rpm for 10 min. Approximately 20 μg of the sample was collected for detection and the same quantity was separated using polyacrylamide gel electrophoresis and sodium dodecyl sulfate before being transferred to a polyvinylidene fluoride membrane. The first antibody was used to incubate the membrane containing the target protein for > 8 h at 4°C and the second antibody was used to cultivate the membrane for 1 h at room temperature. Western blot was detected by chemiluminescence using a Western Blot Assay kit (Yeasen, Shanghai, China).

Bulk RNA-seq analysis

Tumor tissues from three mice in each group were utilized for bulk RNA-seq. RNA-seq analysis was carried out following conventional protocols, which included RNA quantification and

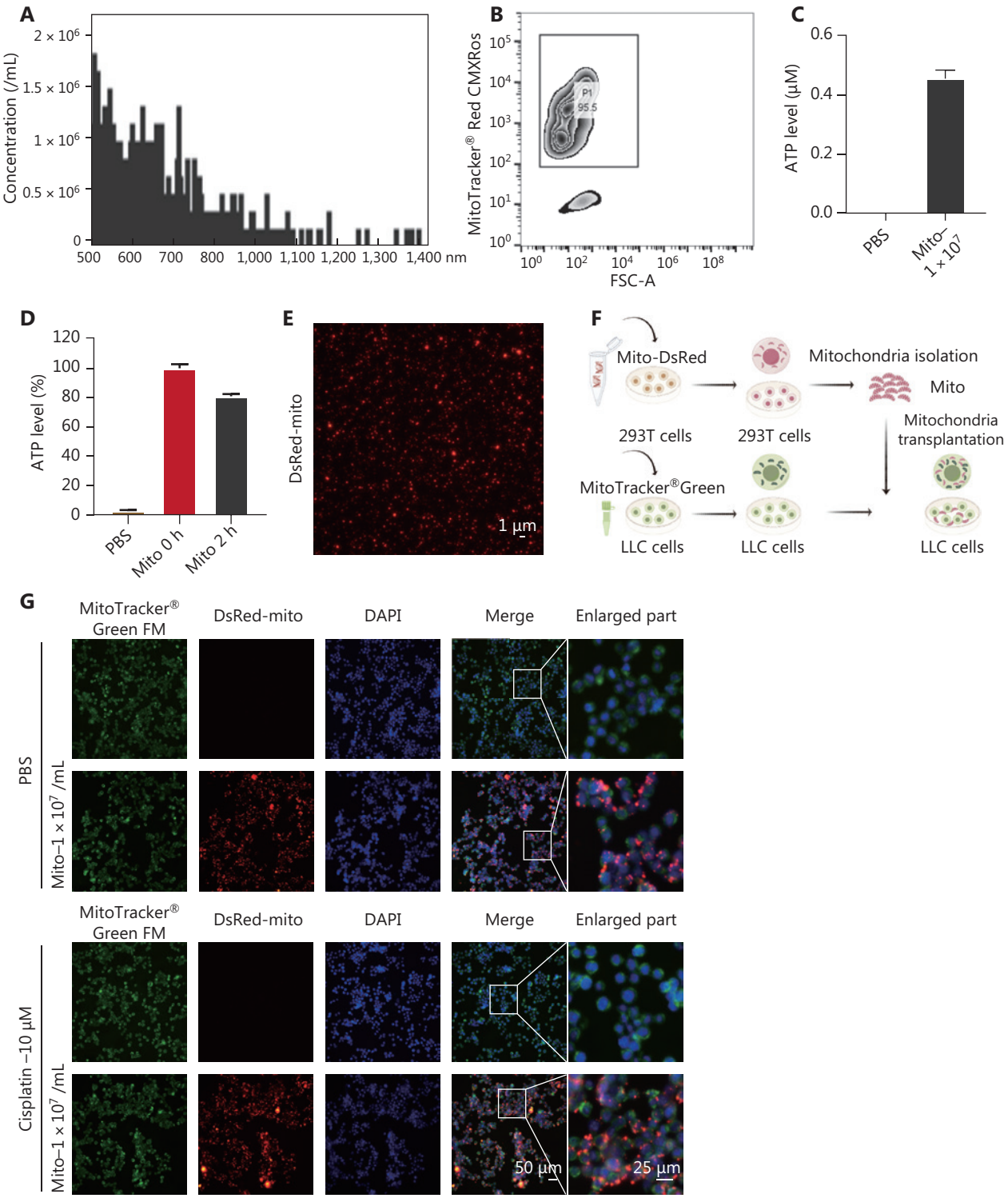


Figure 1 Isolated mitochondria maintain structure and function. (A) A multisizer particle counter was used to quantify the diameters and amounts of the isolated mitochondria. (B) MitoTracker® Red CMXRos staining was utilized to evaluate the viability of the separated mitochondria. (C) ATP content in 1×10^7 mitochondria. (D) Analysis of ATP levels in 2 h and fresh mitochondria. (E) Isolated mitochondria labeled with DsRed were observed *via* fluorescent microscopy. (F) Schematic diagram of the preparation and transplantation of mitochondria. (G) The absorption of co-incubated mitochondria in LLC cells is demonstrated. Scale bars, 25 and 50 μm.

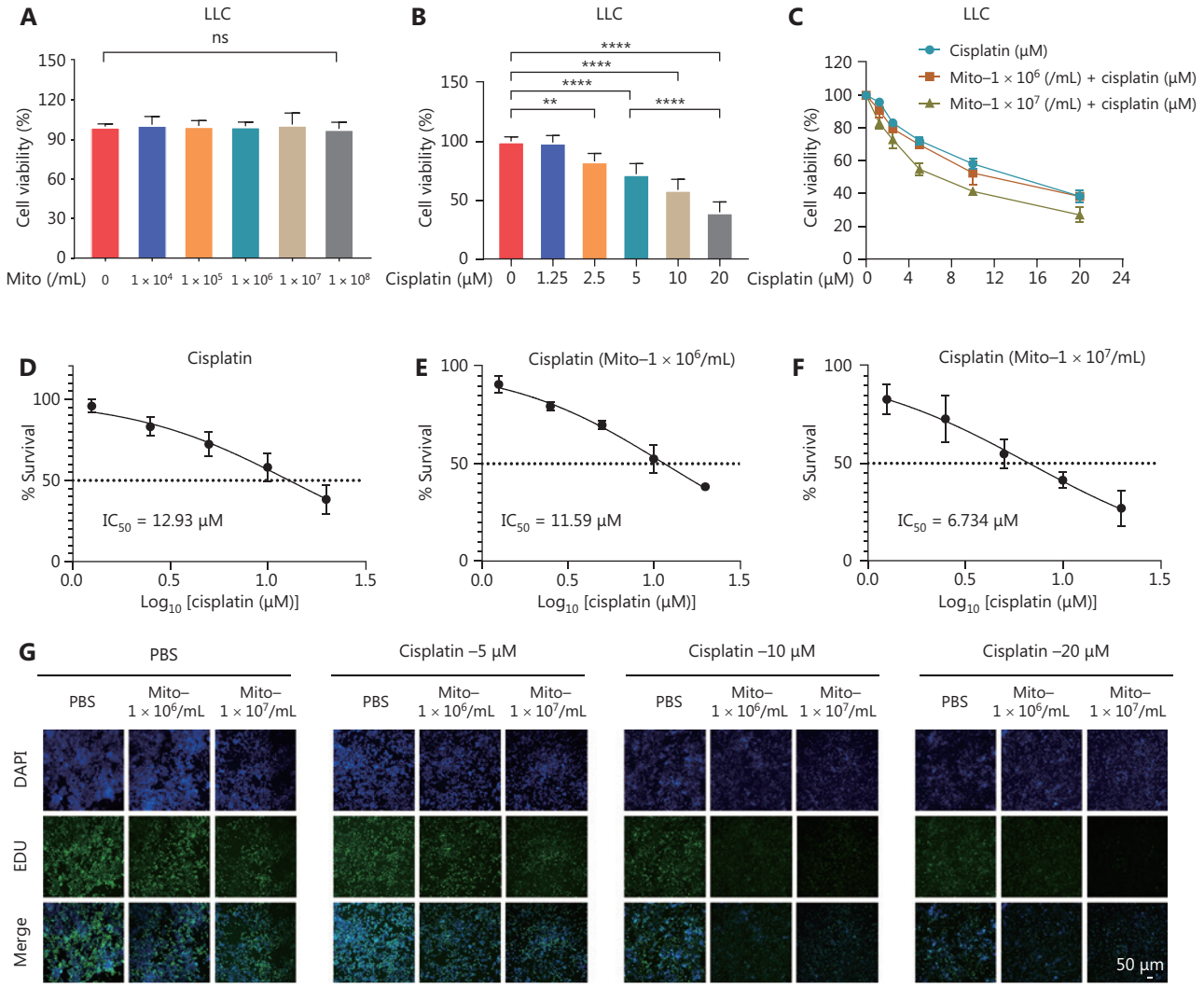


Figure 2 Mitochondrial transplantation enhanced cisplatin sensitivity in LLC cells. (A–C) The viability of LLC cells treated with mitochondrial transplantation alone (A), cisplatin alone (B), and the combination treatment (C) at a series of concentrations was evaluated by CCK-8 assay. (D) The CCK-8 assay measured the cisplatin IC_{50} values. (E, F) The mitochondrial transplantation IC_{50} values at different concentrations combined with cisplatin treatment measured by the CCK-8 assay. (G) EDU staining displayed cell prefoliation in LLC cells after treatment with mitochondrial transplantation alone (1×10^6/mL and 1×10^7/mL), cisplatin alone (5, 10, and 20 μM), and combination treatment. Scale bars, 50 μm. The statistics, which are displayed as a percentage of untreated control cells, are representative of three comparable trials; each point is the mean ± SEM ($n \geq 3$). $^{**}P < 0.01$, and $^{****}P < 0.0001$ compared to the indicated group.

qualification, transcriptome sequencing library preparation, clustering, and sequencing. Differentially expressed gene (DEG) analyses between the case and control groups were performed to gain insight into the change of phenotype. Gene Ontology and Kyoto Encyclopedia of Genes and Genomes (KEGG) enrichment analysis of annotated DEG was performed by Phyper based on hypergeometric testing. Bonferroni adjustment was performed for the significant level of terms and pathways by Q value using a strict threshold (Q value ≤ 0.05).

Measurement of ROS production

The intracellular reactive oxygen species (ROS) level was determined using flow cytometry. Cells were seeded into 6-well plates at a density of 1×10^6 cells/mL. The LLC cells were then transplanted with the specified concentration of mitochondria (1×10^6/mL or 1×10^7/mL) and incubated for 48 h with specified concentrations of cisplatin (5, 10, and 20 μM). The intracellular ROS level was

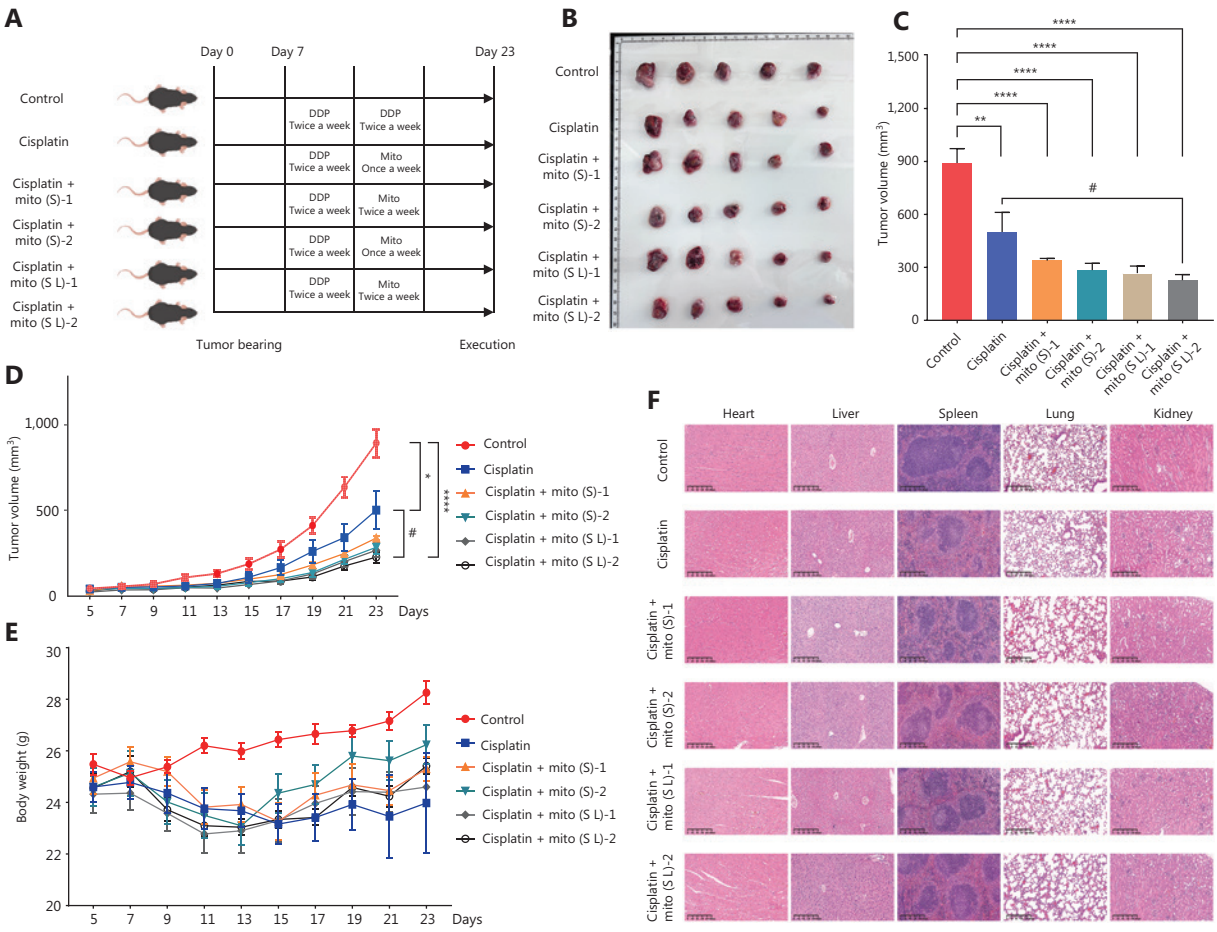


Figure 3 Continued

determined by oxidative conversion of cell permeable 2′, 7′dichlorofluorescein diacetate [DCFH-DA] (Beyotime) to fluorescent dichlorofluorescein (DCF). Following a 30-min incubation period at 37°C with DCFH-DA, the cells were cleaned and subjected to flow cytometry.

TUNEL assay

The TUNEL Assay kit (Roche Diagnostics GmbH, Basel, switzerland) was used to perform the TdT-UTP nick-end labeling (TUNEL) test in accordance with the manufacturer's instructions.

Apoptosis assays

LLC cells with the specified mitochondrial concentrations (1×10^6/mL and 1×10^7/mL) were incubated for 48 h with the specified concentrations of cisplatin (5, 10, and 20 μM). The cells were then washed twice with PBS, digested with 10% trypsin for 2–3 min, and centrifuged for 3 min at 800 rpm. The cells were gently resuspended following removal of the supernatant. After adding 2.5 μL of annexin V-FITC dye diluted with 50 mL of buffer and incubating the cells for 15–20 min at 37°C, the cells were treated for 10 min at 37°C with 5 μL of propidium iodide (PI) dye mixed with 250 μL of buffer. Flow cytometry PI and FITC channels were then used to measure the apoptosis rates for the case and control groups.

Flow cytometry analysis

Mouse tumor tissues were promptly removed for *in vivo* investigations and mechanically separated with scissors in sterile PBS for flow cytometry analysis. Tumor fragments

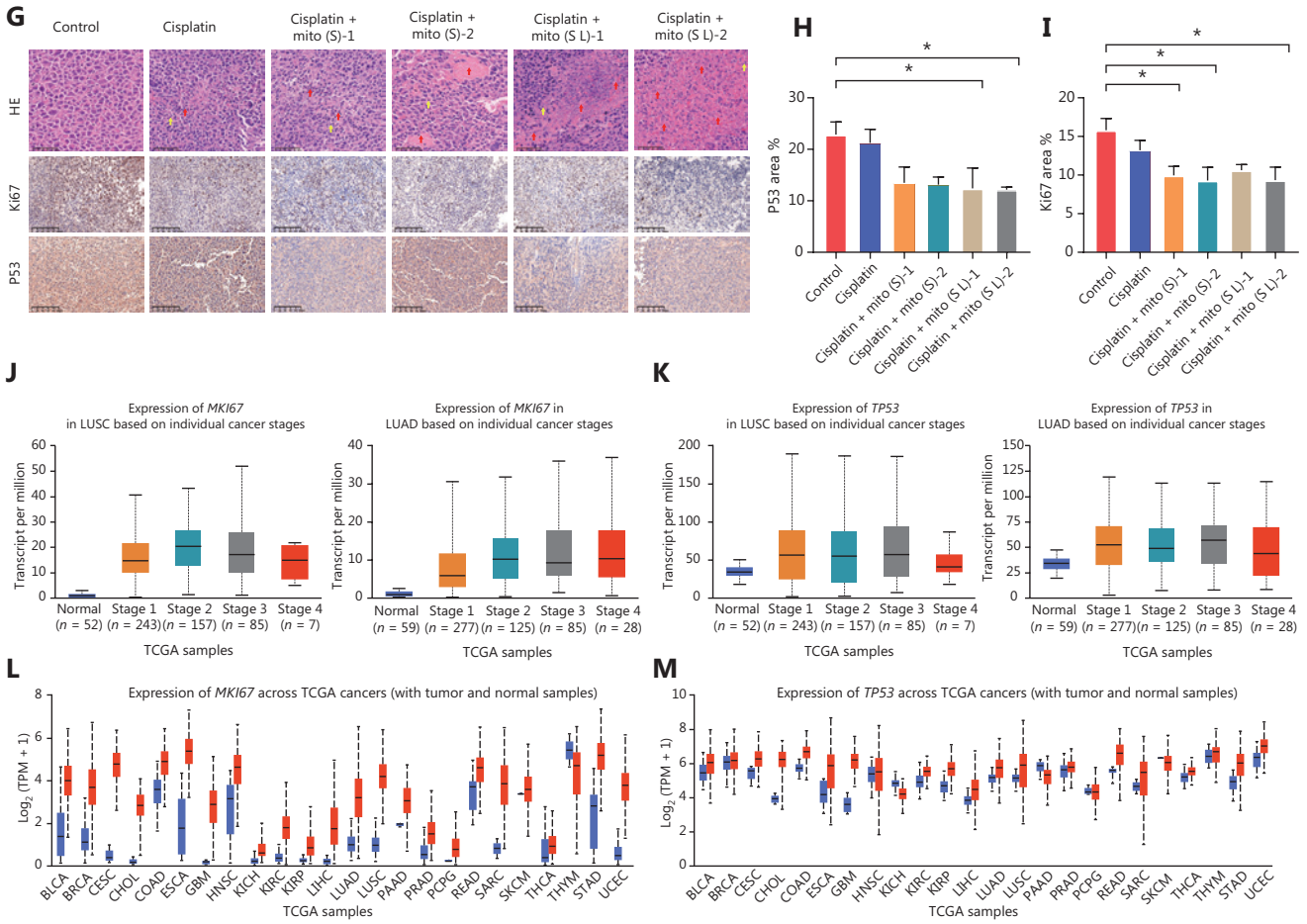


Figure 3 Mitochondrial transplantation suppressed cancer development in LLC cell xenografts. (A) A diagram of the xenograft mouse model and administration schedule. C57BL/6 mice were subcutaneously implanted with LLC cells, then randomized into the following six groups: control group, cisplatin; cisplatin with mito (systemic)-1 [cisplatin + mito (S)-1]; cisplatin with mito (systemic)-2 [cisplatin + mito (S)-2]; cisplatin with mito (systemic and local)-1 [cisplatin + mito (S L)-1]; and cisplatin with mito (systemic and local)-2 [cisplatin + mito (S L)-2]. (B–D) Characteristic pictures of tumors, tumor volumes, and tumor growth curves of C57BL/6 mice from various groups are displayed. (E) Body weight in the six groups of mice described above was statistically analyzed. (F) Typical HE staining images of principal organs in mice treated with various regimens. Scale bars, 200 μm. (G–I) HE and IHC staining of the tumor sections demonstrated the Ki67 and P53 levels in mice treated with various regimens. Scale bars, 50 or 100 μm. (J, K) Expression of *MKI67* and *TP53* in various stages of lung squamous cell carcinoma (LUSC) and lung adenocarcinoma (LUAD) (sequencing data from the TCGA database). (L, M) Expression of *MKI67* and *TP53* in pan-cancer (sequencing data from the TCGA database). $^{*/\#}P < 0.05$, $^{**}P < 0.01$, and $^{****}P < 0.0001$ compared to the indicated group.

were digested in 10% FBS (Biosharp, Hefei, China), 0.5 mg/mL collagenase from *Clostridium histolyticum* type IV (Sigma-Aldrich, MO, USA), 0.15 mg/mL DNase I (RayBiotech, GA, USA), and RPMI-1640 (Biosharp) for 60 min at 37°C with rotation to promote dissociation. Single-cell suspensions were passed through a 70-mm cell strainer. Samples were centrifuged at 300 *g* for 5 min at 4°C. Cells were stained with fluorescently labeled antibodies at a 1:100 dilution in Cell Staining Buffer (RayBiotech, GA, USA) for 30 min at 4°C. Single-cell suspensions were stained with panel 1 (CD45-BV510, CD11b-BUV396, CD3-BV421, CD8a-PerCP-Cy5.5, CD4-FITC, B220-PE-Cy7, and NK1.1-BV605; RayBiotech, GA, USA) and 2 anti-mouse antibodies (CD45-BV510, CD11b-BV786, F480-BUV396, MHC-II-FITC, and CD11c-PE-Cy7; RayBiotech, GA, USA). All data was acquired using a BD LSRFortessa flow cytometer (BD Bioscience) and analyzed with FlowJo software (BD Bioscience, NJ, USA).

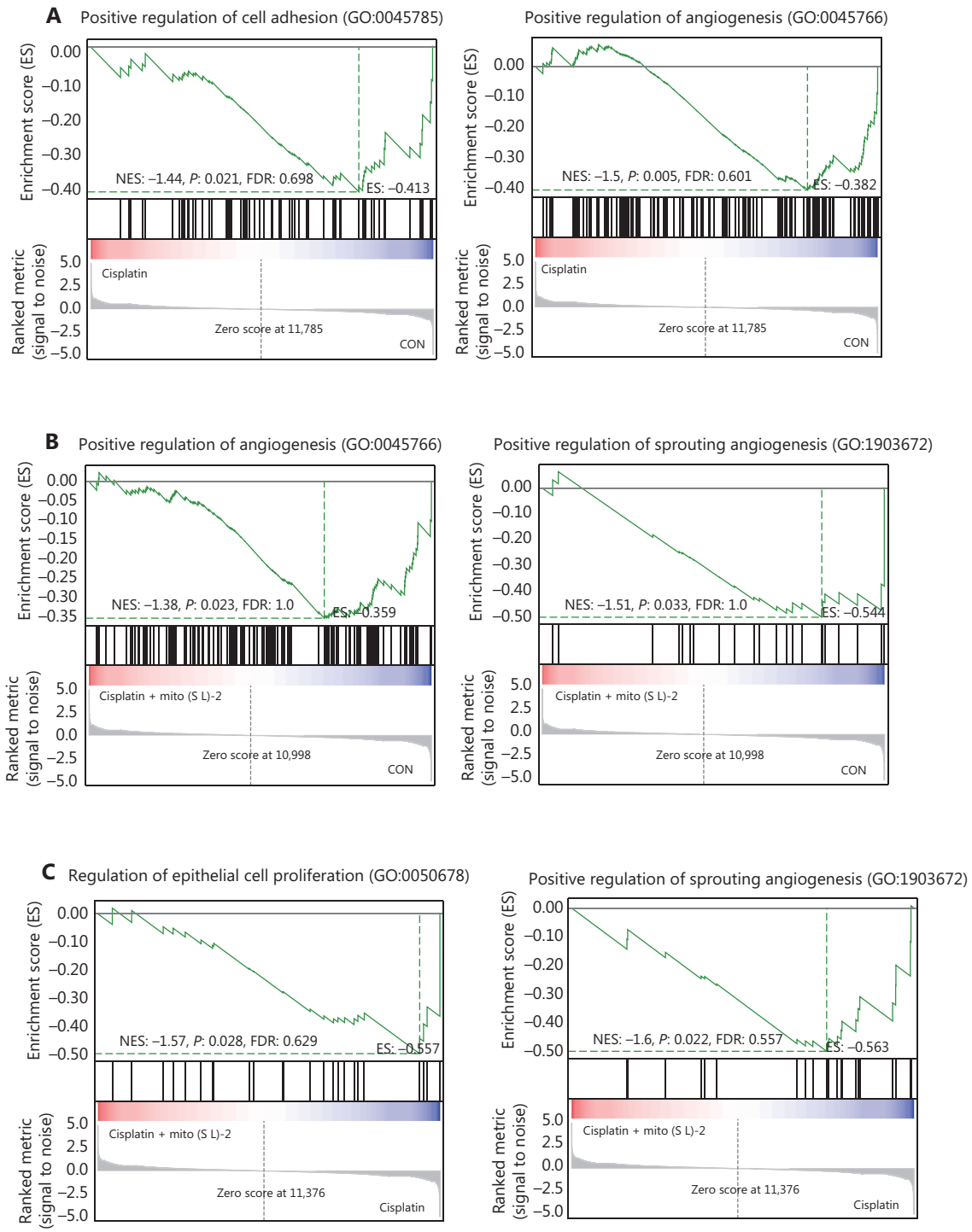


Figure 4 Continued

Sources of population data

Population data were obtained by logging in to the TCGA database, clicking TCGA-LUAD/LUSC data, clicking files, clicking the transcript profiling library ht-seq TPM version of gene expression quantity data, then downloading the cart and metadata files for all patients with lung adenocarcinoma and lung squamous cell carcinoma. Gene sequencing data and

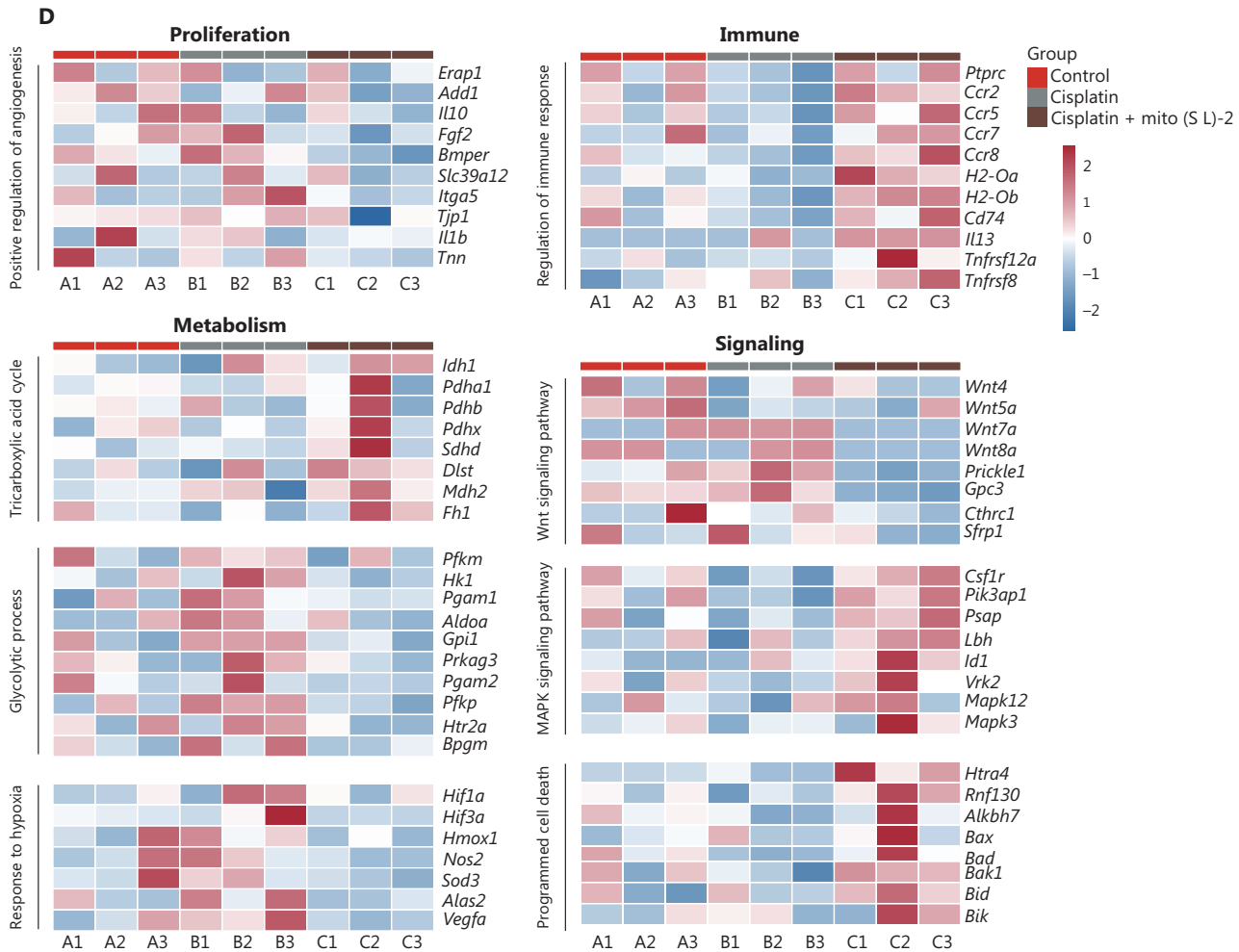


Figure 4 Continued

processed clinical data are contained in the file content. To determine how the target gene is expressed in different types of cancer, the Oncomine Database official website was viewed and the gene was entered directly.

Bioenergetics assessment

The bioenergetic changes caused by mitochondrial transplantation in LLC cells were investigated by measuring the oxygen consumption rate (OCR) using a Seahorse XFe24 analyzer (Agilent, CA, USA). The seeding density was 10,000 LLC cells per well. The optimal drug concentration was 1.5 μm for oligomycin, 1 μm for FCCP, and 2.5 μm for rotenone and antimycin A (R&A). LLC cells were treated with mitochondrial transplantation 24 h later. OCR measurements were performed by sequential treatment with oligomycin, FCCP, and R&A following the Seahorse XFe24 analyzer program.

Cytotoxicity assay

Natural killer (NK) cell-mediated cytotoxicity was assessed according to established methodologies. H460 cells (Chinese Academy of Sciences Cell Bank, Shanghai, China) were infected with eGFP-lentivirus (Hanbio Tech, Shanghai, China). The H460 cells were seeded into 24-well plates and NK92 cells (Chinese Academy of Sciences Cell Bank, Shanghai, China) were pretreated with mitochondrial transplantation for 24 h. Then, NK92 and H460 cells were co-cultured with or without anti-NKP30 antibody (BioLegend, CA, USA). Viable tumor cells were quantified by fluorescence microscopy. T cell-mediated cytotoxicity was assessed according to established

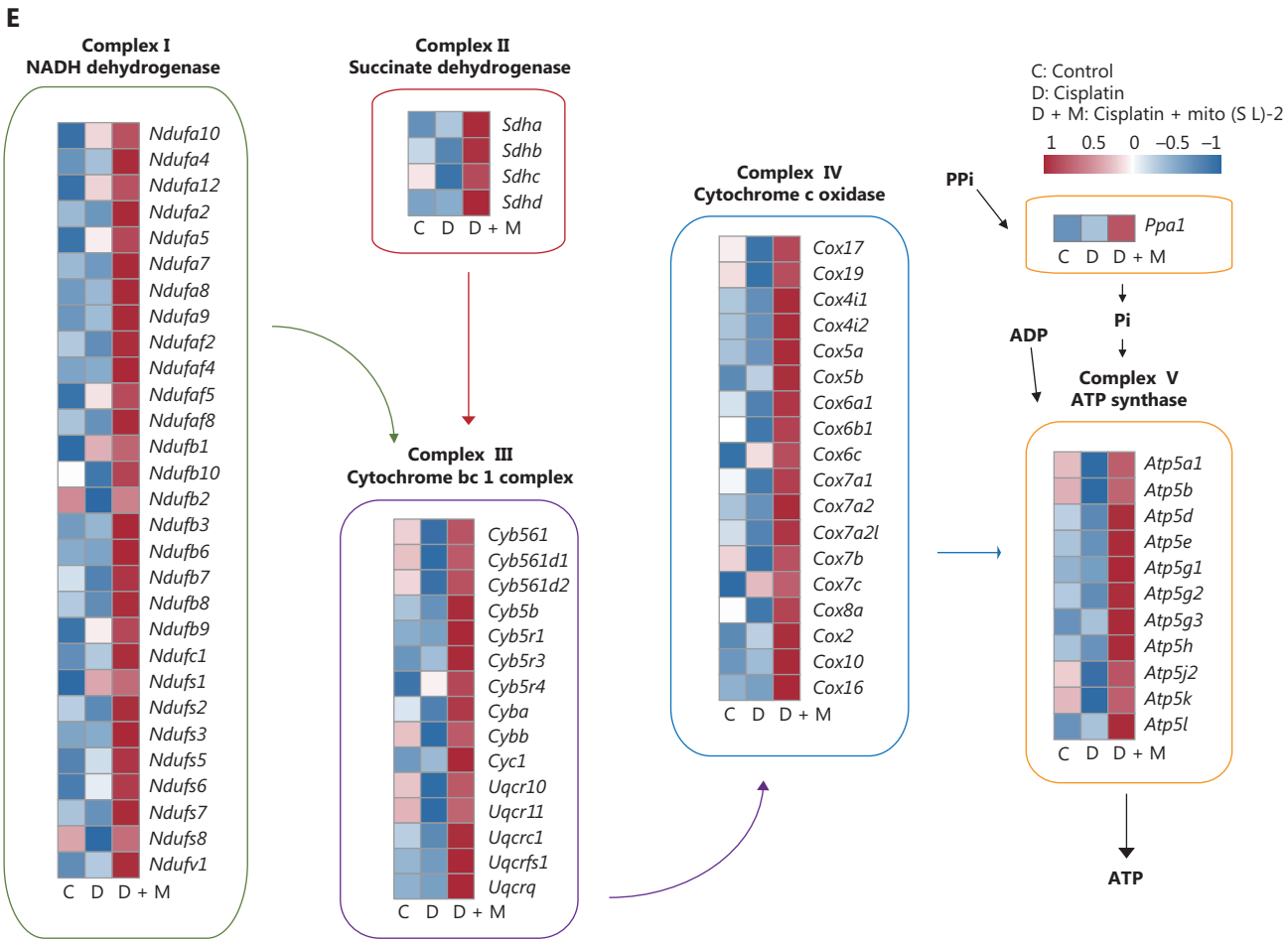


Figure 4 Transcriptomic sequencing analysis of mouse tumor tissues. (A–C) The analysis of GSEA was carried out on tissue samples from mice administered various treatments. The outcomes demonstrated that combination therapy enriched the indicated genomes. (D) Heatmap of transcriptome alterations. Differently expressed genes (DEGs) were detected in tumor specimens in mice administered various regimens. (E) Analysis of transcriptome statistics genes linked to mitochondrial complexes I–V in mouse tissues (FC > 1.2; $P \leq 0.05$).

methodologies. Jurkat-T cells (Chinese Academy of Sciences Cell Bank, Shanghai, China) were pretreated with mitochondrial transplantation for 24 h. Then, H460 cells were co-cultured with Jurkat-T cells (activated with phorbol 12-myristate 13-acetate [PMA]; Sigma-Aldrich, MO, USA and phytohem agglutinin [PHA]; Sigma-Aldrich, MO, USA) with or without anti-CD8 antibody (BioXCell, NH, USA). Viable tumor cells were quantified by fluorescence microscopy.

Statistical analysis

The values are presented as the mean ± SEM and *P* values were generated as listed in the legends. All statistical analyses were performed using GraphPad Prism (v.8.0.1; GraphPad Software, CA, USA). All data are expressed as the mean ± SEM. Comparisons between multiple groups were performed by one-way ANOVA followed by Tukey's multiple comparisons test. A P value < 0.05 was considered statistically significant.

Results

Isolated mitochondria maintain structure and function

Particle size analysis revealed a size range between 0.5 and 1 μm for isolated mitochondria (**Figure 1A**). Mito-Tracker Red CMXRos specifically labels biologically active mitochondria. MitoTracker® Red CMXRos staining and flow cytometry analysis revealed that 95.5% of the mitochondria were viable (**Figure 1B**). The isolated mitochondria were respiratory, as

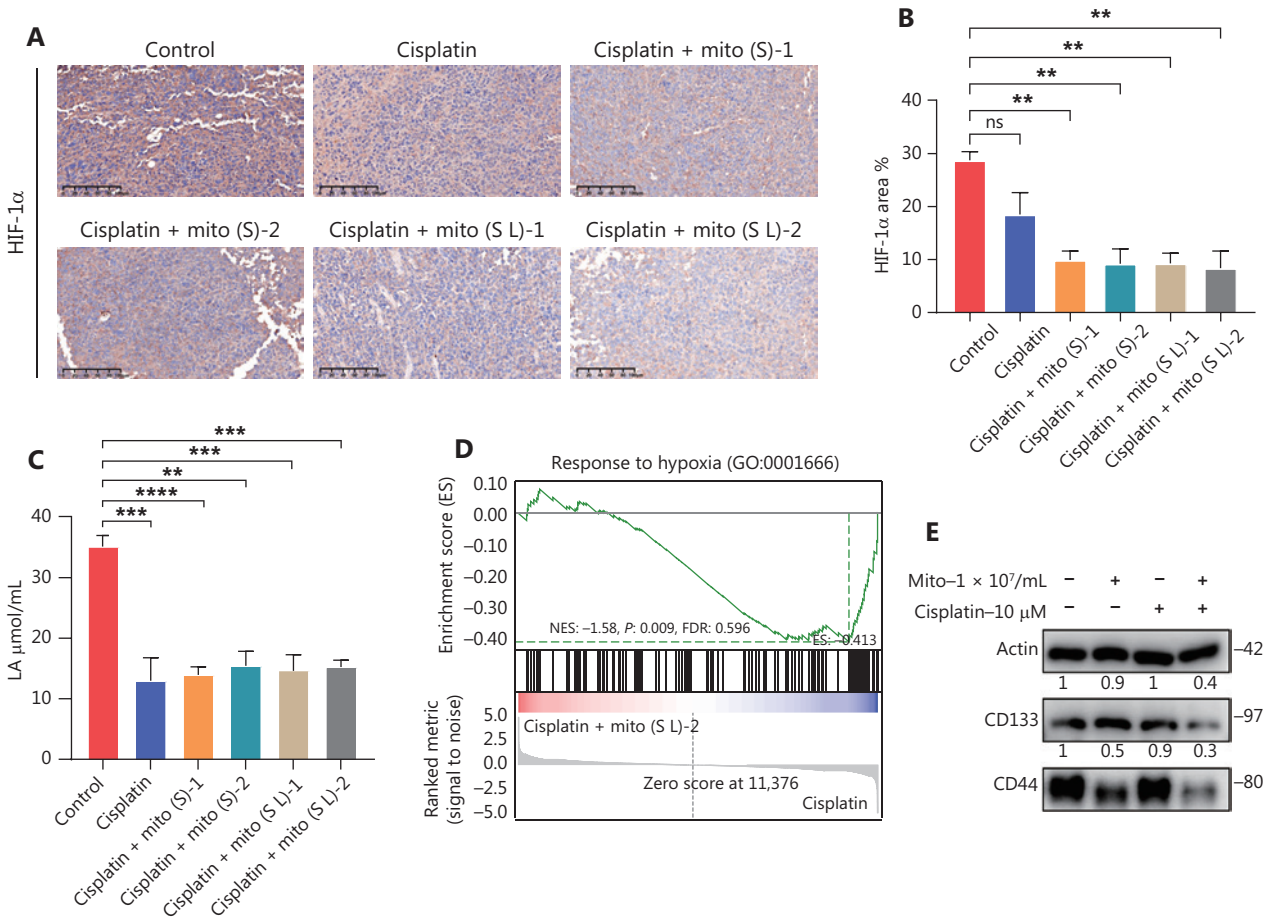


Figure 5 Continued

determined by the ATP level. The ATP level of isolated mitochondria was 0.45 μm for 1 × 10^7 mitochondria (**Figure 1C**). The ATP level of isolated mitochondria after 2 h still reached 81% of fresh mitochondria (**Figure 1D**). These results indicated that the isolated mitochondria were intact, viable, and respiring. 293T cells (Chinese Academy of Sciences Cell Bank, Shanghai, China) were directly transfected with the pCMV-Mito-DsRed-puro lentivirus, which contains the mitochondrial targeting sequence of human cytochrome c oxidase subunit VIII and the codon-optimized red fluorescent protein DsRed gene. This transfection enabled the 293T cells to stably express the Mito-DsRed fusion protein, after which mitochondria were isolated and imaged using a fluorescence microscope (**Figure 1E**). The isolated mitochondria were structurally stable and functional. MitoTracker® Green FM was used to label endogenous mitochondria in LLC cells. We isolated mitochondria as exogenous, functional mitochondria from 293T cells stably expressing the Mito-DsRed fusion protein. LLC cells were co-cultured with DsRed-labeled exogenous mitochondria to determine whether LLC cells could take up exogenous mitochondria. Mitochondrial uptake in LLC cells is shown in **Figure 1G**. Fluorescence microscopy assays revealed that functional mitochondria entered the cells after co-incubation with recipient cells. The co-incubated mitochondria were evenly distributed in the LLC cells and largely located in the cytoplasm (**Figure 1F, G**). Moreover, a mitochondrial stress test was performed that showed the OCR value of LLC cells increased after mitochondrial transplantation. The respiratory function of LLC cells was enhanced after mitochondrial transplantation (**Figure S1**).

Mitochondrial transplantation increased cisplatin sensitivity in LLC cells

According to a previous study, cardiomyocytes demonstrate the highest mitochondrial density among evaluated cell types

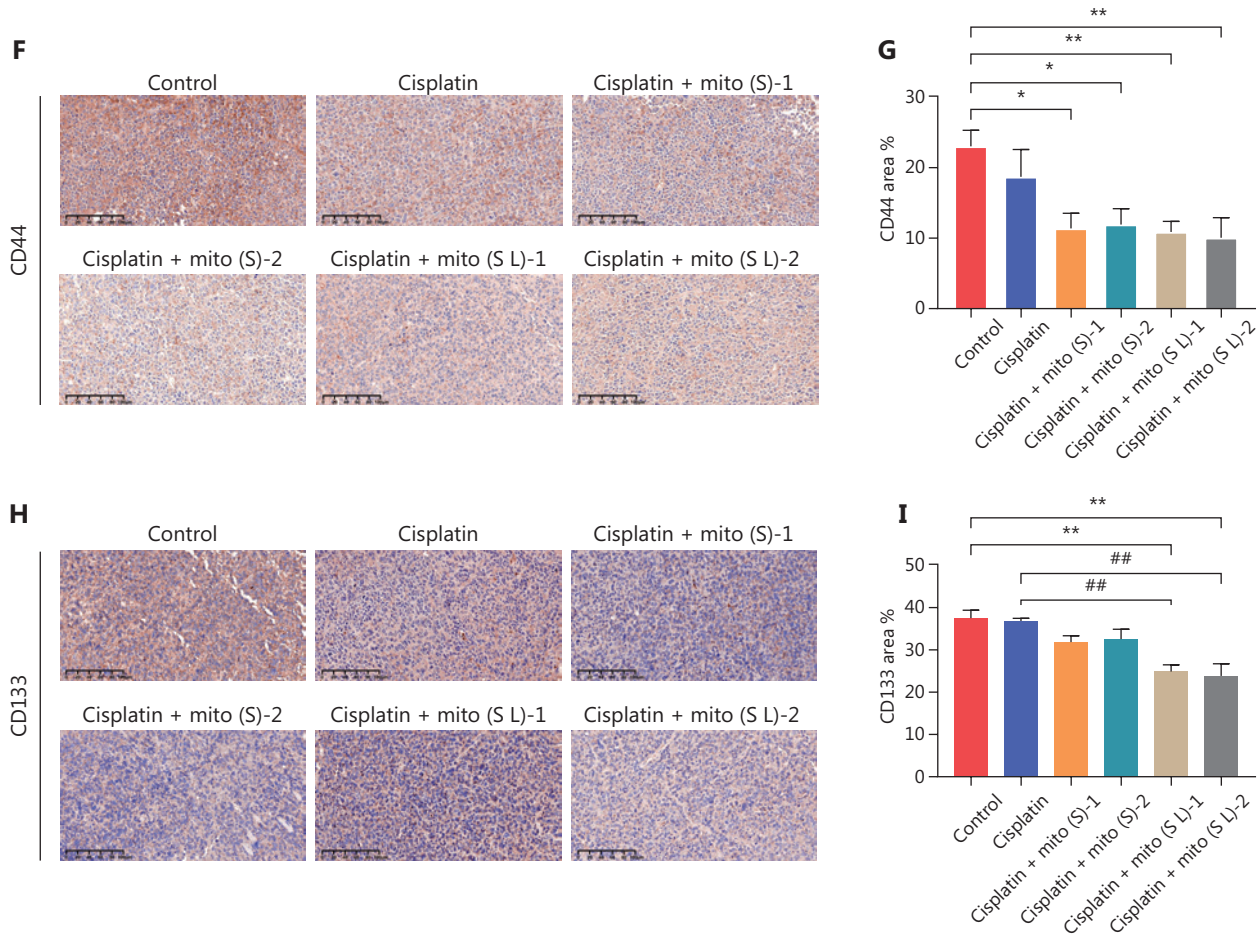


Figure 5 Mitochondrial transplantation reduced tumor stemness by inhibiting HIF-1α. (A, B) IHC showed increased HIF-1α expression in the tumor tissues of mice in each treatment group. Scale bars, 100 μm. Graph B is the quantitative statistics of graph A. (C) The ELISA assay was used to measure the lactic acid level in tumor tissues. (D) The results of GSEA analysis confirmed enrichment of the gene sets associated with response to hypoxia in tumor tissues. (E) Western blotting displayed the amounts of CD44 and CD133 protein in LLC cells. (F–I) The IHC assays demonstrated the level of CD44 (F, G) and CD133 (H, I) in mice administered various treatments. Scale bars, 100 μm. *P < 0.05, **/##P < 0.01, ***P < 0.001 and ****P < 0.0001 compared to the indicated group.

with significantly elevated OCRs and enhanced ATP generation capacity. Notably, the mitochondrial functional efficiency remains superior, as evidenced by ATP production levels second only to embryonic stem cells (ESCs), even after mitochondrial volume normalization, indicating robust mitochondrial biogenesis and exceptional bioenergetic competence. Therefore, AC16 cells (a type of cardiomyocyte) were selected as the mitochondrial donor source in the present study[14]. Next, cytotoxicity of different concentrations of mitochondria in LLC cells was determined using CCK-8 assays. After a 48-h co-incubation, the viability of LLC cells remained unaffected by transplantation of mitochondria alone at concentrations ranging from 1×10^4/mL to 1×10^8/mL (**Figure 2A**). Next, the cytotoxicity of cisplatin in LLC cells was determined at 48 h using CCK-8 assays. Cisplatin impaired cell viability in a dose-dependent manner with an IC_{50} value of 12.93 μM (**Figure 2B, D**). Combinations of mitochondrial transplantation at concentrations of 1×10^6/mL or 1×10^7/mL and cisplatin treatment further enhanced cisplatin cytotoxicity, which was confirmed by a decrease in the cisplatin IC_{50} value (**Figures 1C, 2E, F**). A combination of cisplatin with 1×10^7/mL mitochondrial transplantation reduced the cisplatin IC_{50} to 6.7 μM (**Figure 2F**). In subsequent experiments, 5 and 10 μM cisplatin were utilized as low and high doses, respectively, and mitochondria were transplanted at a concentration of 1×10^7/mL. EdU incorporation assays were performed following co-incubation of cells with cisplatin and mitochondria transplantation at 1×10^7/mL to study cell proliferation, which

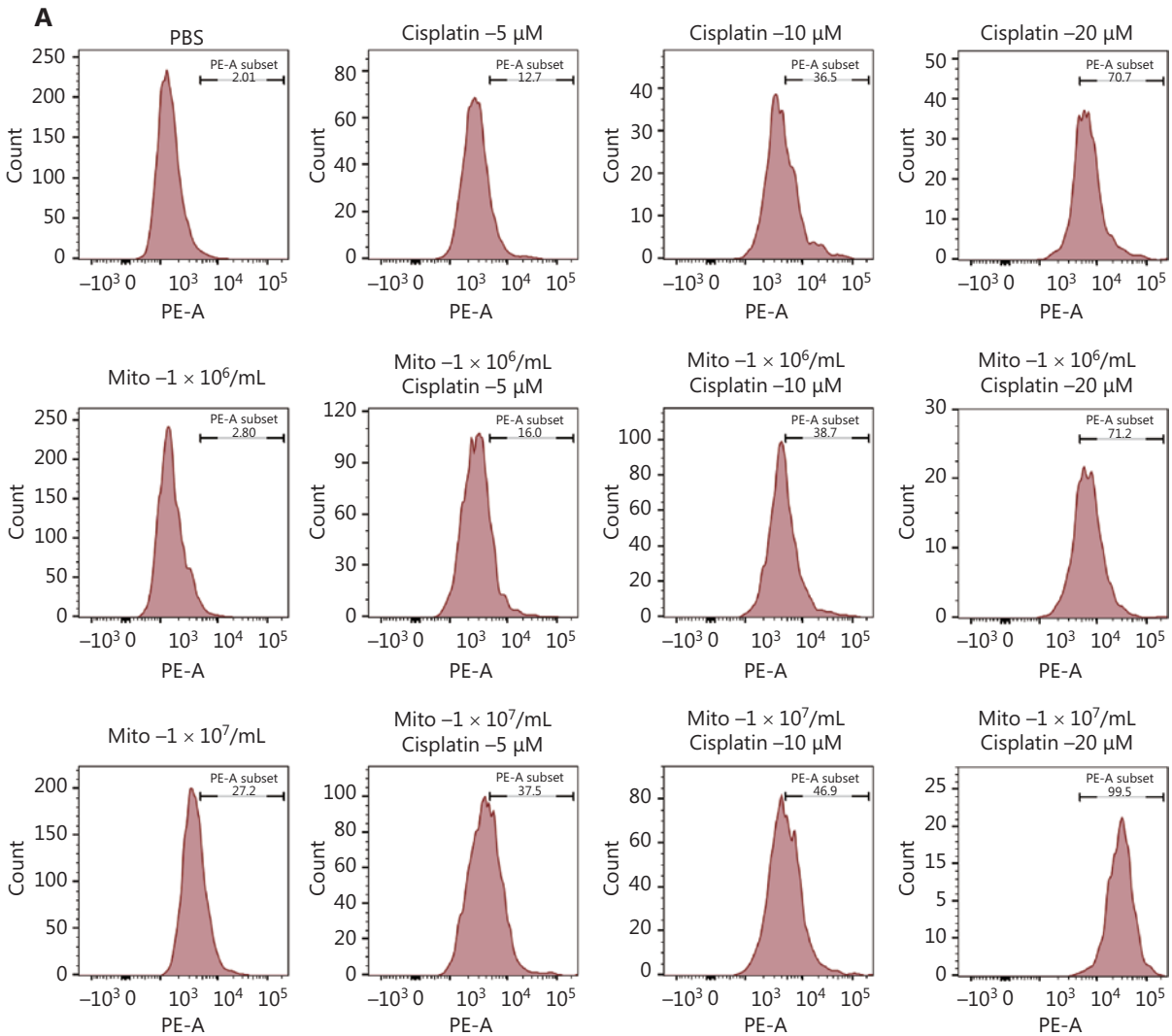


Figure 6 Continued

revealed significant growth inhibition compared to invasively growing LLC cells (**Figure 2G**).

Overall, the results illustrated that mitochondria remained morphologically intact and viable and could further potentiate the cytotoxic effect of cisplatin *in vitro*.

Mitochondrial transplantation decreased tumor growth in LLC cell xenografts

The mechanism contributing to the combined mitochondrial transplantation and cisplatin treatment on tumor growth was elucidated using *in vivo* experiments with subcutaneous tumor models. The schematic illustration is displayed in **Figure 3A**. C57BL/6 mice were inoculated subcutaneously with LLC cells (1×10^6 cells) in the right flank. The tumor volume was measured using a caliper at baseline and after a 3-week recovery period; the measurements are shown in **Figure 3D**. Tumor growth was significantly suppressed following cisplatin treatment or a combination of cisplatin and mitochondrial transplantation (**Figure 3B, C**). The combination of cisplatin with two mitochondrial transplants (systemic and local) caused a significant shrinkage in LLC tumor volumes compared to cisplatin treatment alone based on caliper measurements (**Figure 3B, C**). No significant differences in body weight were detected among LLC tumor-bearing mice or between groups (**Figure 3E**). H&E staining demonstrated no significant anatomic alterations in the heart, liver, spleen, lung, or kidney tissues (**Figure 3F**). These results demonstrated that none of the treatments significantly

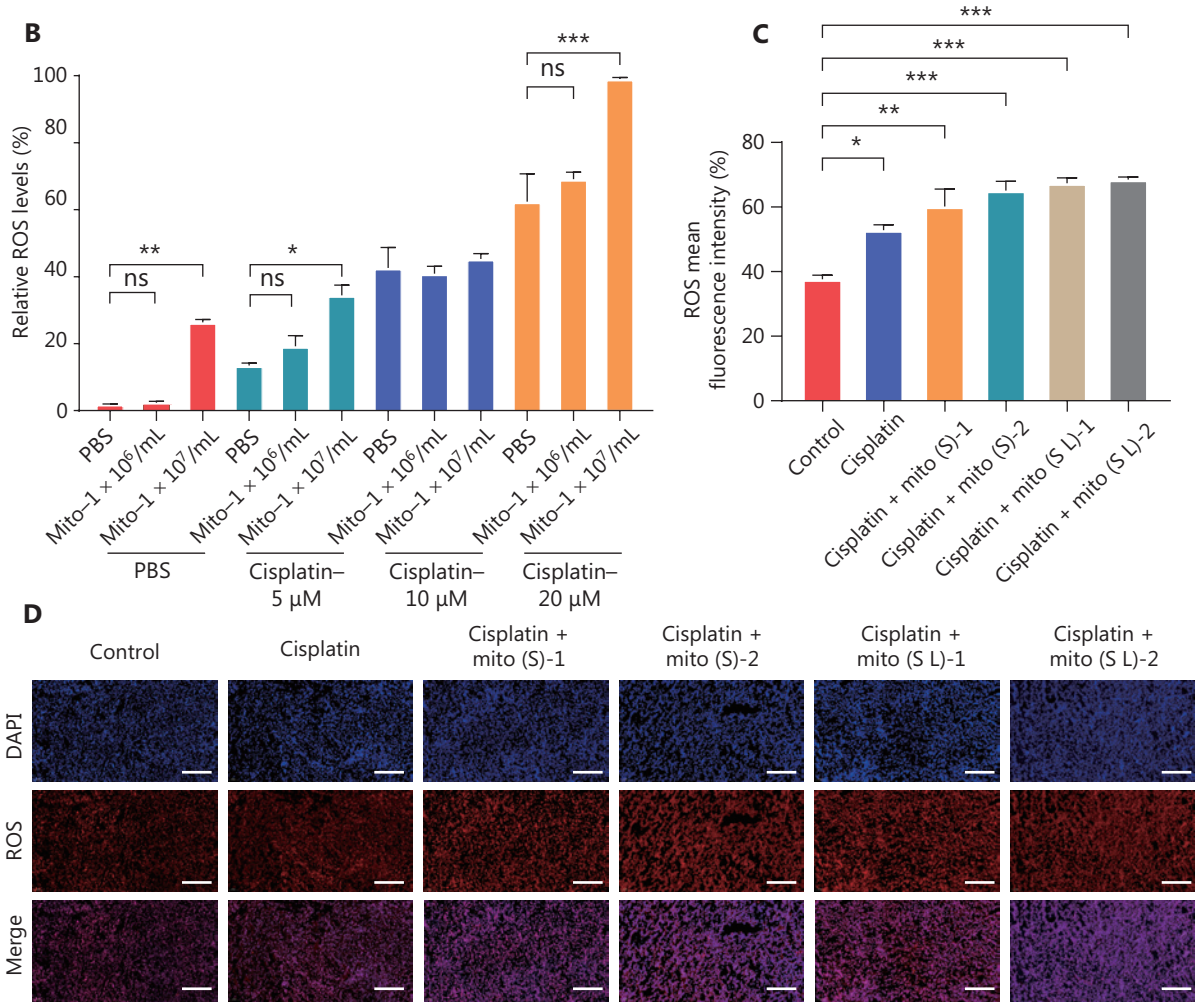


Figure 6 Continued

impacted the nutritional status or toxicity. H&E staining revealed that part of the tumor cells in the visual field were necrotic, the nuclei disappeared, the cytoplasm was stained red (indicated by the red arrow), and the tissue was infiltrated by individual inflammatory cells (indicated by the yellow arrow) compared to the control group, (**Figure 3G**). Immunohistology staining revealed decreased cell proliferation, which was consistent with tumor growth detected in the animal model. Compared to the LLC control group, considerable downregulation of Ki67 and P53 expression was noted in the cisplatin with mitochondrial transplantation treatment group (**Figure 3G-I**). The TCGA sequencing database shows that *MKI67* and TP53 are abundantly expressed in different stages of lung squamous cell carcinoma (LUSC) and lung adenocarcinoma (LUAD) (**Figure 3J, K**). Furthermore, *TP53* and *MKI67* are substantially expressed in a range of malignancies (**Figure 3L, M**).

The mechanism underlying the delay in tumor progression was further elucidated by a combination of mitochondrial transplantation and cisplatin chemotherapy. Systematic transcriptome sequencing analysis of murine tumor tissues was performed. The cisplatin treatment group, especially the mitochondrial transplantation combined with cisplatin group, resulted in a series of changes in gene expression that were largely concentrated in with respect to cell proliferation, anti-tumor immune responses, tumor metabolism, and tumor malignancy-related signaling pathways compared to the control group. First, co-treatment with mitochondrial transplantation and cisplatin significantly downregulated the expression of tumor angiogenesis-related genes, thus enriching anti-tumor immune responses, including T cells, NK cells, and antigen presentation. Second, normally differentiated cells largely depend on oxidative phosphorylation of

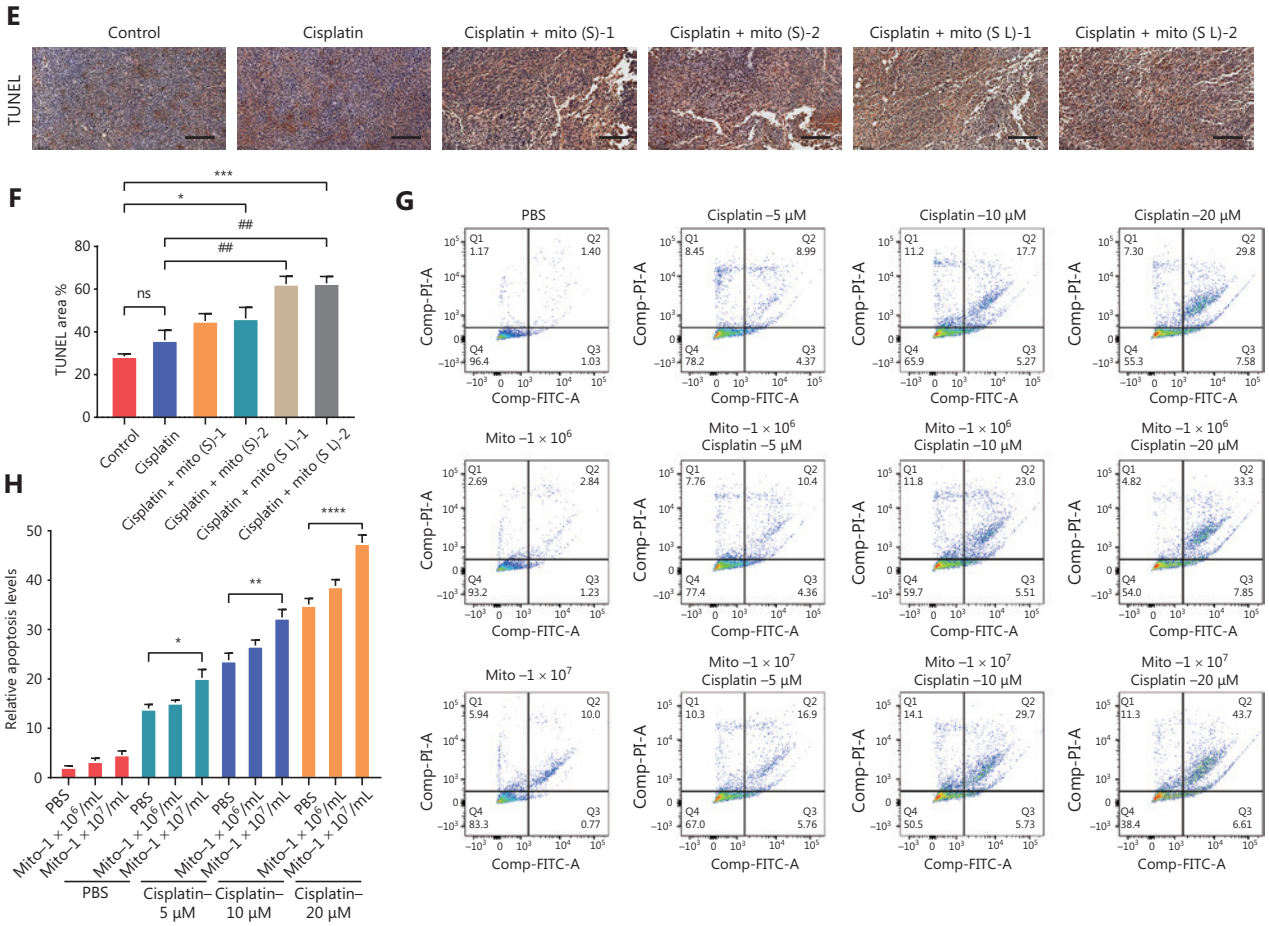


Figure 6 Continued

mitochondria for the cell energy supply, whereas most tumor cells depend on aerobic glycolysis, a phenomenon known as the Warburg effect. The Warburg effect is one of the primary metabolic characteristics of tumor cells. Transcriptomic analysis revealed that mitochondrial transplantation combined with cisplatin significantly downregulated glycolysis and expression of hypoxia response genes in tumor cells and significantly upregulated the expression of tricarboxylic acid cycle-related genes, implying that the combined treatment altered the metabolic reprogramming of tumor cells. Finally, the pathways related to tumor cell apoptosis (the MAPK signaling pathway and programmed cell death) were significantly upregulated in the combined treatment group, whereas the pathways related to tumor malignancy (Wnt signaling pathway) were significantly inhibited (**Figure 4A-D**). Further analysis demonstrated that the combination treatment with mitochondrial transplantation and cisplatin significantly upregulated mitochondrial oxidative phosphorylation pathway complexes I–V (Nduf, Sdhb, Cycb, Cyc1, Uqcr, Cox, Ppa1, and Atp5 families). These results further demonstrated that mitochondrial transplantation plus cisplatin altered the metabolic reprogramming of the tumor and the metabolic type of tumor from the Warburg effect to oxidative phosphorylation (**Figure 4E**). The above findings revealed that mitochondrial transplantation combined with cisplatin chemotherapy reversed tumor metabolic reprogramming and enhanced anti-tumor immunity, which suppressed tumor cell proliferation and accelerated tumor cell apoptosis.

Mitochondrial transplantation reduced tumor stemness by inhibiting HIF-1α

HIF-1α is particularly prevalent in different tumors and is correlated with tumor invasion, metastasis, and angiogenesis[14-16]. IHC staining was performed on murine tumor tissues, the results of which demonstrated that HIF-1α was significantly

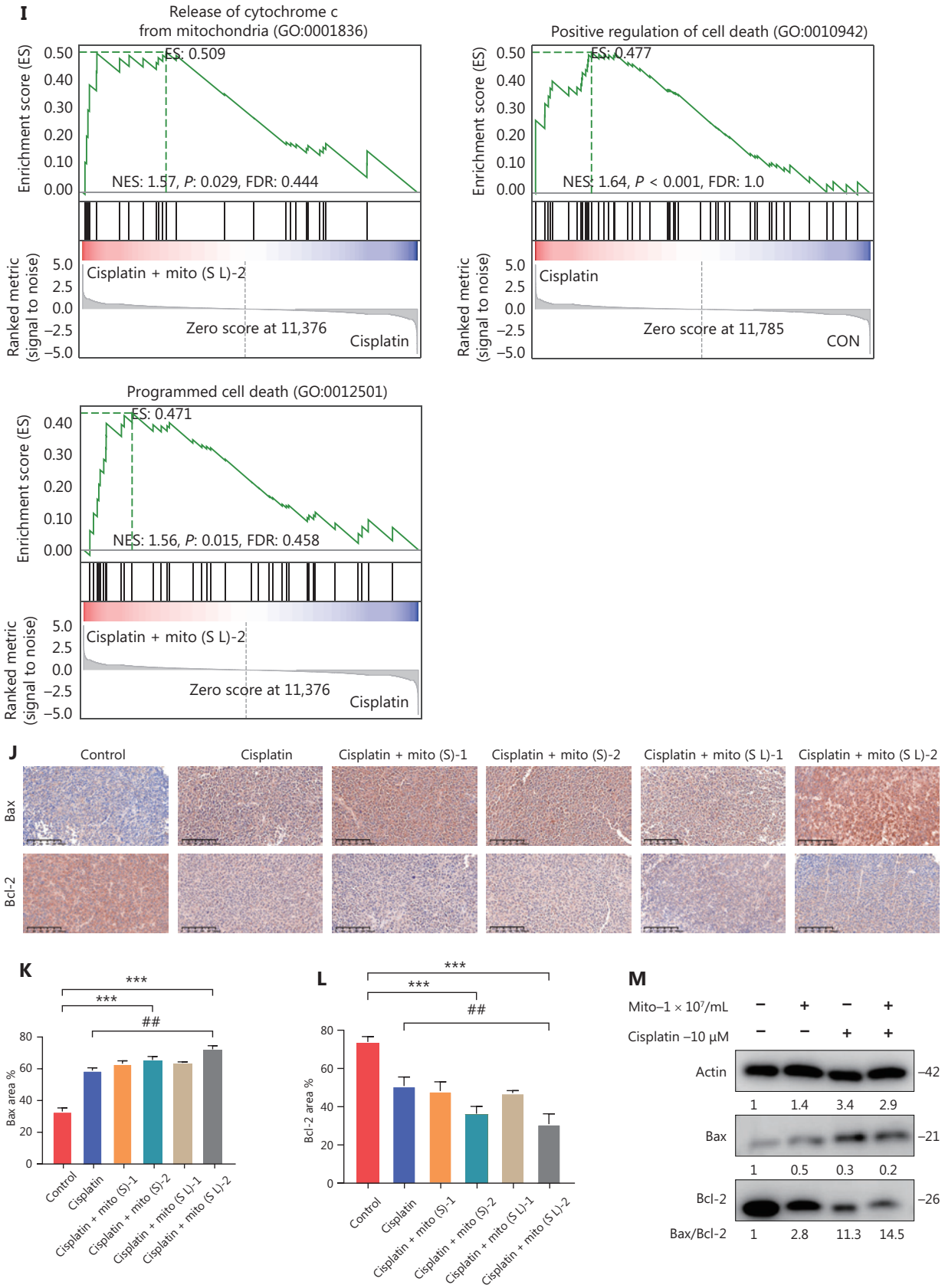


Figure 6 Continued

Figure 6 Mitochondrial transplantation led to ROS elevation and induced mitochondria-related apoptosis. (A, B) Flow cytometry demonstrated the ROS level in LLC cells that were untreated or received cisplatin, mitochondrial transplantation, or a combination of treatments. (C, D) Immunofluorescence revealed the amount of ROS in tumor tissues. Scale bars, 100 μm. (E, F) TUNEL assays for apoptosis in mice tumor tissues administered different treatments. Scale bars, 100 μm. (G, H) Flow cytometry demonstrated the apoptosis level in LLC cells that were untreated or received cisplatin, mitochondrial transplantation, or a combination of treatments. (I) The results of GSEA analysis indicated enrichment of the gene sets associated with programmed cell death. (J, K) IHC staining demonstrated the amount of Bax and Bcl-2 in tumor tissues from mice. Scale bars, 100 μm. (M) Western blotting showed the amount of Bax and Bcl-2 in LLC cells that were exposed to different treatments. *P < 0.05, **/##P < 0.01, ***P < 0.001 and ****P < 0.0001 compared to the indicated group.

downregulated in the cisplatin group, especially in the mitochondrial transplantation combined with cisplatin group, compared to the control group (**Figure 5A, B**). Tumor hypoxia and glycolysis are the primary causes of chemotherapy failure. Glycolysis produces abundant lactic acid. The accumulation of lactic acid in the tumor microenvironment accelerates tumor growth[17,18]. Therefore, the lactic acid content in murine tumor tissues was determined. Lactic acid in the combined mitochondrial transplantation and cisplatin group was significantly reduced compared to the cisplatin group (**Figure 5C**). Transcriptome sequencing results revealed that the hypoxic response was significantly downregulated following co-treatment with mitochondrial transplantation and cisplatin compared to cisplatin treatment alone (**Figure 5D**). HIF-1α upregulation is known to increase tumor stemness[19-21]. The mitochondria and cisplatin combination suppressed CD133 and CD44 expression *in vitro*, as detected by western blotting (**Figure 5E**). IHC staining on murine tumor tissues demonstrated that CD44 and CD133 expression was greatly diminished in the cisplatin alone group, especially in combination with mitochondrial transplantation and cisplatin (**Figure 5F-I**). Taken together, mitochondrial transplantation combined with cisplatin chemotherapy reduced tumor stemness by inhibiting the hypoxic response.

Mitochondrial transplantation led to ROS elevation and induced mitochondria-related apoptosis

Specific stages of carcinogenesis can be effectively halted by increasing oxidative damage and enhancing ROS-dependent death signals. ROS accumulation results in different forms of cell death and senescence[22,23]. Flow cytometry confirmed a significantly elevated ROS level in LLC cells after cisplatin intervention that was even more substantial after co-treatment with cisplatin and mitochondrial transplantation (**Figure 6A, B**). This conclusion was further confirmed by *in vivo* experiments, which demonstrated that the ROS level increased dramatically upon cisplatin intervention and even more extensively upon cisplatin combined with mitochondrial transplantation intervention (**Figure 6C, D**). Apoptosis pathways can be divided into endogenous mitochondrial, endogenous endoplasmic reticulum, and exogenous death receptor pathways[24]. Internal apoptotic stimuli, such as activation of oncogenes, DNA damage, cell hypoxia, and loss of cell growth factors, can activate the mitochondrial apoptotic pathway in cells and cause apoptosis[25]. Whether mitochondria paired with cisplatin treatment improved tumor apoptosis was determined by performing TUNEL staining on murine tumor tissues. The results showed that combination treatment with cisplatin and mitochondrial transplantation markedly induced tumor apoptosis compared to all other groups (**Figure 6E, F**). Flow cytometry demonstrated a significant increase in apoptosis of LLC cells after cisplatin intervention, which was further amplified by the combination of cisplatin and mitochondrial transplantation (**Figure 6G, H**). Transcriptomic analyses revealed significantly upregulated apoptosis signal of cancer cells *in vivo* after cisplatin intervention; combination with mitochondrial transplantation further enhanced the release of mitochondrial cytochrome c and facilitated cancer cell apoptosis (**Figure 6I**). IHC staining of murine tumor tissues demonstrated significant downregulation of Bcl-2 and upregulation of Bax in the cisplatin group compared to the control group, especially in the mitochondrial transplantation combined with cisplatin group (**Figure 6J-L**). This result was further validated in *in vitro* cellular experiments by western blotting (**Figure 6M**). Taken together, these findings demonstrated that mitochondrial transplantation elevates ROS production and induces mitochondria-related apoptosis.

Mitochondrial transplantation by inhibiting Wnt/β-catenin signaling pathway promoted tumor immune infiltration

T-cell versatility is a hallmark of protective immunity against cancer. Studies have reported that Wnt activation inhibits the differentiation of human memory CD8+T cells and promotes

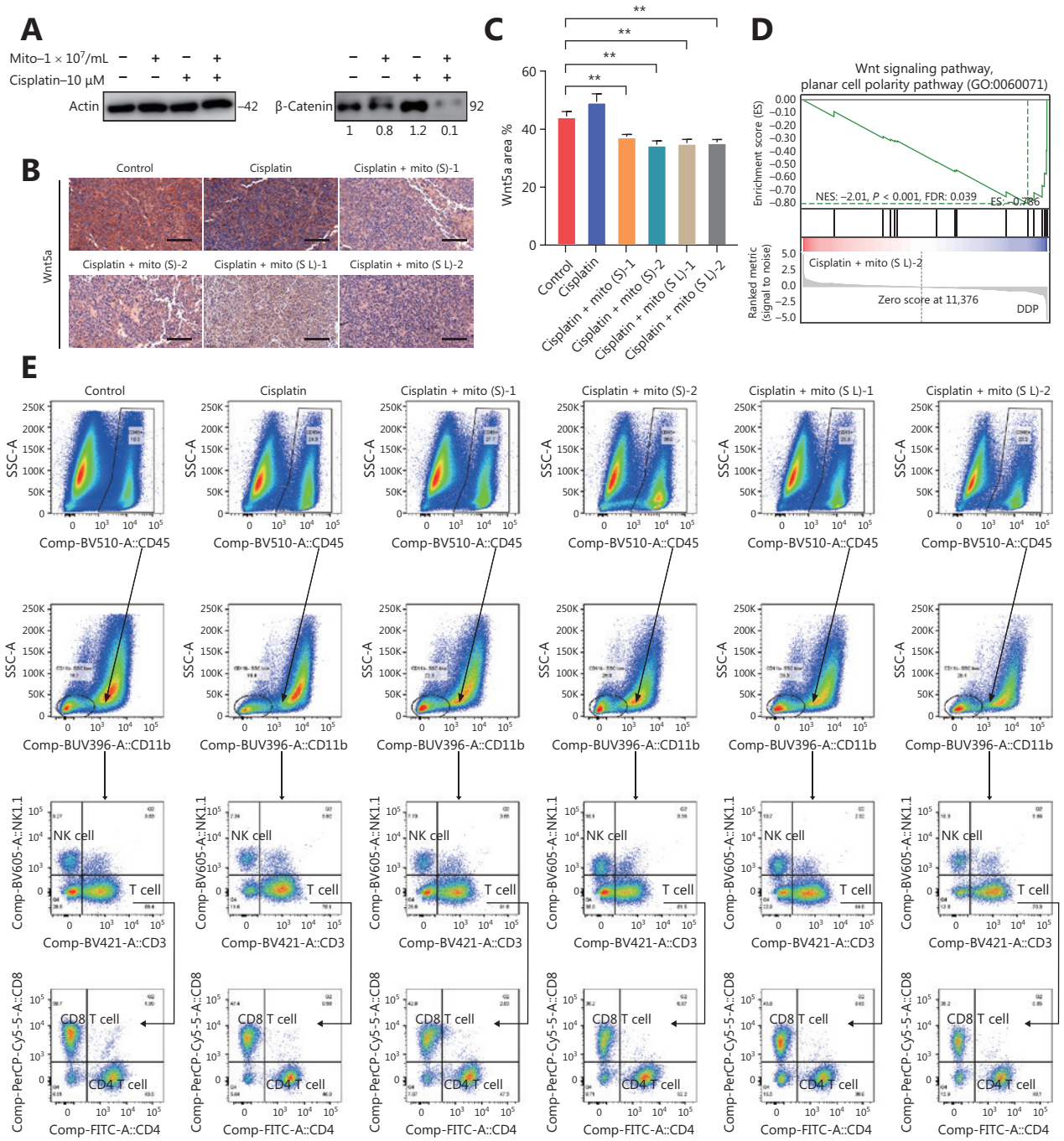


Figure 7 Continued

(TME). To elucidate the immunomodulatory effects of mitochondrial transplantation on immune cell-mediated antitumor responses, an *in vitro* co-culture system using human NK92 and H460 cells was established with or without mitochondrial transplantation. Quantitative analysis revealed that mitochondrial transplantation significantly enhanced the tumoricidal activity of NK92 cells against H460 targets, as evidenced by increased cytotoxicity. However, antibody-mediated depletion of NK cells substantially attenuated mitochondrial-induced enhancement concomitant with impaired tumor cell lysis (**Figure S5A, B**). Then, the experiments demonstrated that mitochondrion transplantation similarly potentiated Jurkat

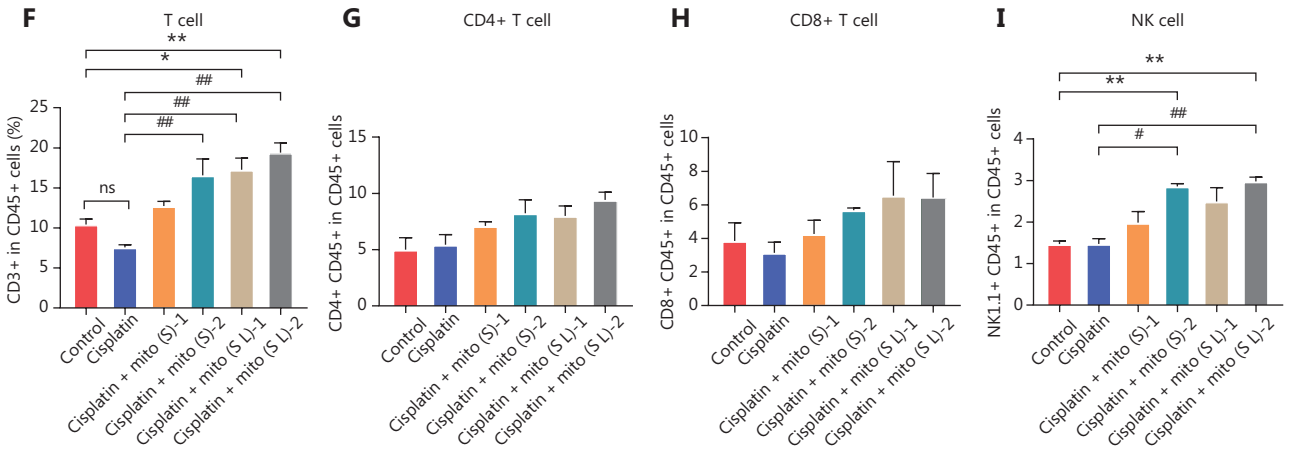


Figure 7 Mitochondrial transplantation by inhibiting Wnt signaling pathway promoted tumor immune infiltration. (A) Western blotting displayed the β-catenin level in LLC cells treated with cisplatin, mitochondria, or a combination. (B, C) The IHC assay showed the amount of Wnt5a in mice treated with different exposures. Scale bars, 50 μm. (D) The results of GSEA analysis confirmed enrichment of the gene sets associated with the Wnt signaling pathway. (E–I) Flow cytometry investigation of immune cell subsets in malignancies. Characteristic flow cytometry diagrams exhibiting NK cells, CD3+ T cells, CD4+ T cells, and CD8+ T cells in the tumors of mice undergoing various therapies. NK cells (I), CD3+ T cells (F), CD4+ T cells (G), and CD8+ T cells (H) as a percentage of tumors in mice undergoing various therapies. $^{*/\#}P < 0.05$ and $^{**/\#\#}P < 0.01$ compared to the indicated group.

the production of highly multifunctional cells[26,27]. NSCLC inhibits the infiltration of T cells in tumors in a Wnt/β-catenin signaling pathway-dependent manner, followed by inhibition of the anti-tumor immune response[28,29]. The combination of cisplatin (10 μM) and mitochondria (1×10^7/mL) dramatically suppressed the Wnt/β-catenin signaling pathway in LLC cells. Western blotting demonstrated that the combination of mitochondria and cisplatin substantially diminished β-catenin expression *in vitro* (**Figure 7A**). IHC staining of mouse tumor tissues demonstrated that Wnt5a expression in the mitochondrial transplantation combined with cisplatin group was significantly inhibited compared to the control group (**Figure 7B, C**). Transcriptome sequencing analysis revealed considerable suppression of Wnt signaling pathway in the mitochondrial transplantation plus cisplatin when compared to the cisplatin alone treatment (**Figure 7D**). effect of mitochondrial transplantation and cisplatin on immune infiltration of advanced NSCLC was further investigated using flow cytometry and IHC staining analysis to detect tumor tissues in all groups of mice. The findings demonstrated significantly elevated T-cell immune infiltration in the tumors of mice treated with mitochondrial transplantation plus cisplatin. However, tumors of mice treated with cisplatin alone failed to demonstrate any measurable difference. Similarly, NK cell infiltration was considerably elevated in the combination therapy group (**Figures 7E-I, 8A-E**). However, B cells, macrophages, and dendritic cells showed little differences among the groups (**Figures S2-S4**).

Next, the changes in tumor immune-related functions during mitochondrial plus cisplatin for advanced NSCLC were determined. Transcriptomics analysis was performed on tumors in each group, followed by functional enrichment of different genes in each group. Chemotherapy is often accompanied by immune cell reduction and other adverse effects. Genomic enrichment analysis (GSEA) revealed that cisplatin chemotherapy impaired T-cell activation, NK cell-mediated cytotoxicity, innate immunity, and adaptive immunological responses. Nevertheless, cisplatin in conjunction with mitochondrial transplantation boosted the following: T cell activation, differentiation, and processing; antigen presentation and processing; exogenous antigen peptide antigen processing and presentation; NK cell-mediated cytotoxicity; NK cell activation; and adaptive immune response modulation (**Figure 8F-H**). These results demonstrated that cisplatin alone impairs tumor immune infiltration. However, a combination of mitochondrial transplantation and cisplatin significantly enhanced tumor immune infiltration.

Functional exhaustion of NK cells and cytotoxic T lymphocytes (CTLs) represents a pivotal mechanism underlying tumor immune evasion in the tumor immune microenvironment

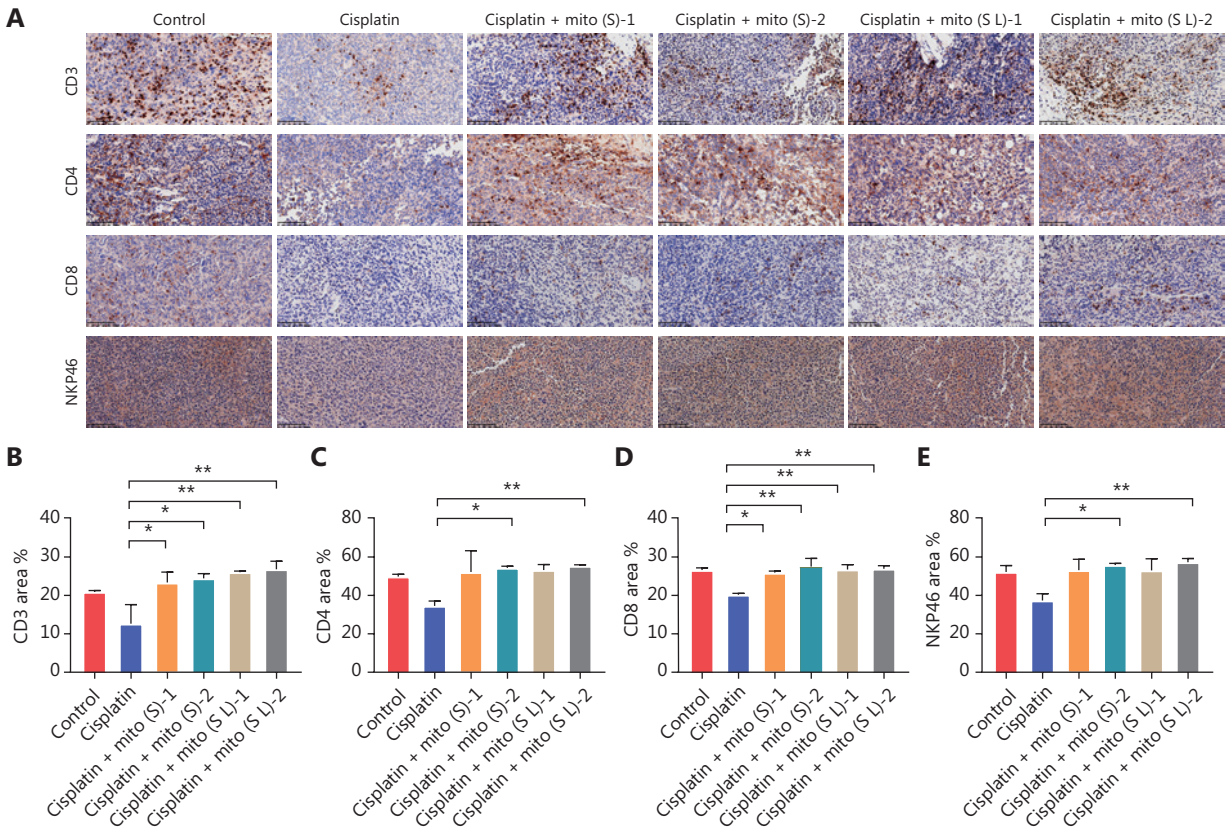


Figure 8 Continued

T-mediated killing of H460 cells and this immunostimulatory effect was markedly diminished following T cell-depletion (**Figure S5C, D**). These experimental findings demonstrated that mitochondrion transplantation significantly enhances the tumoricidal activity of T cells and NK cells.

Discussion

In recent years significant advances and progress have occurred in lung cancer treatment. However, drug resistance is still the major reason for treatment failure in patients with cancer[30-32]. Patients may become resistant to first-line drugs and the efficacy of treatment is greatly reduced[33]. In addition, 40%–80% of all patients with cancer are estimated to be receiving chemotherapy with platinum-containing drugs and patients with chemotherapy resistance have an extremely poor survival rate[34-37]. Several studies have suggested that the development of cancer, including the subsequent emergence of chemotherapy resistance, is intricately related to mitochondria. Mitochondrial transplantation promises to be an effective treatment for several diseases, including cancer[38-40].

The effect of a combination of mitochondrial transplantation and chemotherapy *vs.* chemotherapy alone was determined to investigate the therapeutic potential of mitochondrial transplantation in lung cancer. Mitochondrial transplantation alone did not reduce the viability of LLC cells (**Figure 2A**). In contrast, low-dose cisplatin administration in combination with mitochondrial transplantation dramatically reduced LLC cell viability. This reduction was equal to that obtained with high-dose cisplatin therapy alone (**Figure 2C-F**). *In vivo* experiments using LLC cancer cells were performed to further demonstrate that mitochondrial transplantation dramatically improves chemotherapeutic sensitivity (**Figure 3C**). Cisplatin is a commonly applied chemotherapeutic for this type of malignancy. *In vivo* investigations validated the *in vitro* findings. One week of cisplatin combined with mitochondrial transplantation therapy resulted in or even outperformed 2 weeks of cisplatin. Transcriptomics analysis corroborated these findings, which demonstrated that mitochondrial transplantation

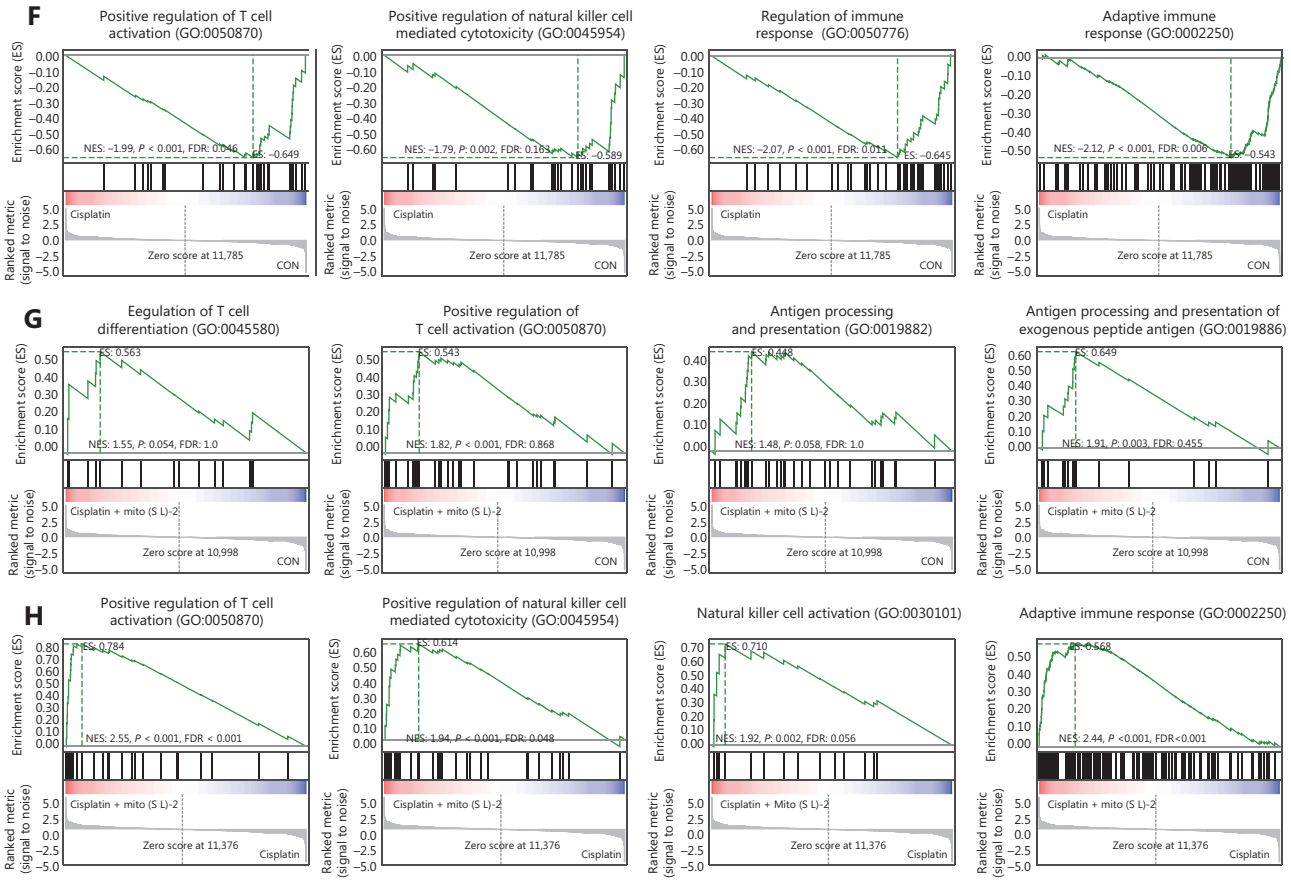


Figure 8 Mitochondrial transplantation promoted tumor immune infiltration. (A–E) The IHC assay displayed the expression of CD3, CD4, CD8, and NKP46. Scale bars, 100 μm. IHC staining quantification is displayed below. (F–H) The results of GSEA analysis demonstrated enrichment of genomes associated with T and NK cell-mediated immune responses. *P < 0.05 and **P < 0.01 compared to the indicated group.

in conjunction with cisplatin considerably boosts inflammatory cell infiltration in tumor grafts and significantly reduces angiogenesis and total cancer cell proliferation (**Figure 4**). We hypothesize that mitochondrial transplantation can overcome cisplatin resistance. However, more research is warranted to verify this theory.

Previous studies have demonstrated that HIF-1α upregulation enhances tumor stemness[41]. The findings of the current study revealed that cisplatin reduces the expression of HIF-1α in LLC cells and significantly downregulates the expression of CD44 and CD133, especially in the combined mitochondrial transplantation and cisplatin group (**Figure 5**). We speculate that mitochondrial transplantation reverses cisplatin resistance by inhibiting HIF-1α and reducing tumor stemness. Maintaining homeostasis of ROS, an important by-product of cellular metabolism[42-44], is essential for cancer cell survival[45,46]. Tumor stem cells, like normal tissue stem cells, have a low level of ROS, which may promote stem cell self-renewal and enhance drug resistance[47,48]. Cisplatin was shown to increase ROS in LLC cells, especially in the combined mitochondrial transplantation and cisplatin group, and also disrupted rROS homeostasis in tumors (**Figure 6D**). In addition, mitochondrial transplantation in combination with chemotherapy was shown to dramatically promote apoptosis of LLC cells, primarily observed as enhanced late apoptosis (**Figure 6E**). Thus, a combination of mitochondrial transplantation with cisplatin increased the production of ROS, ultimately promoting mitochondria-related apoptosis of LLC cancer cells.

Although chemotherapy is the most common treatment option for lung cancer, chemotherapy alone often results in inevitable drug resistance, thereby reducing drug efficacy[49]. The continuous progress and breakthroughs in lung cancer treatment have led to the emergence of cancer immunotherapy targeting tumor-specific T cells, especially reactivation of

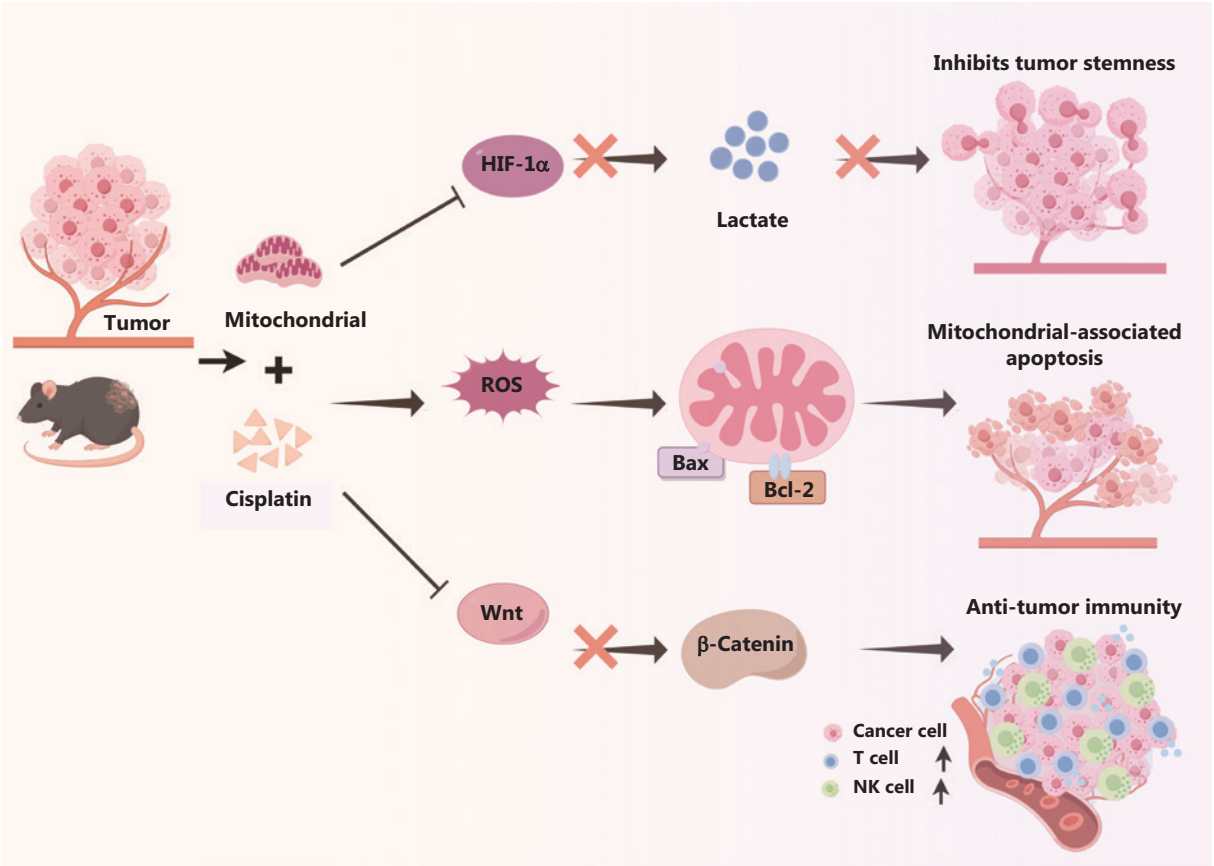


Figure 9 The schematic diagram illustrates the synergistic anti-tumor effect of the combination of mitochondrial transplantation and cisplatin. Mitochondrial transplantation combined with cisplatin inhibited tumor stemness by diminishing HIF-1α and reducing lactate accumulation. Mitochondrial transplantation plus cisplatin triggered the ROS-mediated mitochondrial apoptotic pathway. The combination of mitochondrial transplantation and cisplatin boosted T and NK cell-mediated anti-tumor immunity by preventing the Wnt/β-catenin pathway to inhibit tumor development. Representations shown in **Figure 9** were created with figdraw.com.

CD8+ T cells to promote antitumor immunity, offering hope and clinical promise[50].

Some studies have reported that tumor cells can hijack the mitochondria to support growth[12]. Inhibiting the formation of nanotubes to prevent tumor cells from hijacking mitochondria is a newly emerging anti-tumor therapy. Intercellular mitochondrial transfer enhances CD8+ T cell bioenergetic capacity, tumor penetration, and anti-tumor effects[13]. Animal experiments have demonstrated that a combination of mitochondrial transplantation and cisplatin treatment can significantly improve tumor immune infiltration of LLC tumor-bearing mice and overcome the shortcomings of cisplatin, including damage to lymphocytes and a reduction in the number of immune cells (**Figure 7E**). Moreover, transcriptomics has revealed that the combination of mitochondrial transplantation and cisplatin treatment significantly enriches anti-tumor immune responses, including T cells, NK cells, and antigen presentation (**Figure 8F-H**). These results demonstrated that mitochondrial transplantation combined with cisplatin not only significantly improves the function of tumor-infiltrating immune cells but also significantly promotes the infiltration of immune cells to tumor tissues, thereby activating the anti-tumor immune response (**Figure 9**).

Conclusions

We found for the first time that the effect of 1 week of cisplatin combined with mitochondrial transplantation was better than 1 weeks of cisplatin in *in vivo* experiments in mice, achieving the goal of reducing the number of chemotherapy sessions in 1 week. In addition, mitochondrial transplantation combined with cisplatin significantly improved the immune infiltration of advanced NSCLC, overcoming the shortcomings of cisplatin,

such as myeloid cell damage and immune cell reduction (**Figure 8**). This study put forward beneficial propositions for improving immune infiltration and enhancing the anti-tumor effect during chemotherapy for advanced NSCLC. Furthermore, this study provided substantial support for mitochondrial transfer as a new paradigm for tumor therapy as well as a new direction for future improvements in organelle therapy.

Grant support

This work was supported by the National Natural Science Foundation of China (Grant No. 81922030), the International Cooperation Project of the Belt and Road (Grant No. 20400750600), the Construction Project of Shanghai TCM-integrated Innovative Flagship Hospital [Grant No. ZY (2021-2023)-0205-05, ZXXT-202203], and the Shanghai Municipal Commission of Health and Family Plan (Grant No. 201840056).

Conflict of interest statement

No potential conflicts of interest are disclosed.

Author contributions

Conceived and designed the analysis: Shumeng Lin, Liuliu Yuan and Lihong Fan.
Collected the data: Shumeng Lin, Liuliu Yuan, Xiao Chen and Shiyin Chen.
Contributed data or analysis tools: Mengling Wei, Bingjie Hao and Tiansheng Zheng.
Performed the analysis: Shumeng Lin, Liuliu Yuan, Xiao Chen and Shiyin Chen.
Wrote the paper: Shumeng Lin, Liuliu Yuan, Xiao Chen and Shiyin Chen.

Data availability statement

The data that support the findings of this study are available from the corresponding author upon reasonable request.

References

1. Bray F, Laversanne M, Sung H, Ferlay J, Siegel RL, Soerjomataram I, et al. Global cancer statistics 2022: GLOBOCAN estimates of incidence and mortality worldwide for 36 cancers in 185 countries. CA Cancer J Clin. 2024; 74: 229-63.
2. Siegel RL, Miller KD, Wagle NS, Jemal A. Cancer statistics, 2023. CA Cancer J Clin. 2023; 73: 17-48.
3. Miller KD, Fidler-Benaoudia M, Keegan TH, Hipp HS, Jemal A, Siegel RL. Cancer statistics for adolescents and young adults, 2020. CA Cancer J Clin. 2020; 70: 443-59.
4. Dasari S, Tchounwou PB. Cisplatin in cancer therapy: molecular mechanisms of action. Eur J Pharmacol. 2014; 740: 364-78.
5. Liu Z, Yu Z, Chen D, Verma V, Yuan C, Wang M, et al. Pivotal roles of tumor-draining lymph nodes in the abscopal effects from combined immunotherapy and radiotherapy. Cancer Commun (Lond). 2022; 42: 971-86.
6. Klemm F, Joyce JA. Microenvironmental regulation of therapeutic response in cancer. Trends Cell Biol. 2015; 25: 198-213.
7. Passaro A, Al Bakir M, Hamilton EG, Diehn M, André F, Roy-Chowdhuri S, et al. Cancer biomarkers: emerging trends and clinical implications for personalized treatment. Cell. 2024; 187: 1617-35.
8. Revesz IA, Joyce P, Ebert LM, Prestidge CA. Effective γδ T-cell clinical therapies: current limitations and future perspectives for cancer immunotherapy. Clin Transl Immunology. 2024; 13: e1492.
9. Mammucari C, Rizzuto R. Signaling pathways in mitochondrial dysfunction and aging. Mech Ageing Dev. 2010; 131: 536-43.
10. Jin X, Liu D, Kong D, Zhou X, Zheng L, Xu C. Dissecting the alternation landscape of mitochondrial metabolism-related genes in lung adenocarcinoma and their latent mechanisms. Aging (Albany NY). 2023; 15: 5482-96.
11. Lucà S, Zannini G, Morgillo F, Della Corte CM, Fiorelli A, Zito Marino F, et al. The prognostic value of histopathology in invasive lung adenocarcinoma: a comparative review of the main proposed grading systems. Expert Rev Anticancer Ther. 2023; 23: 265-77.
12. Saha T, Dash C, Jayabalan R, Khiste S, Kulkarni A, Kurmi K, et al. Intercellular nanotubes mediate mitochondrial trafficking between cancer and immune cells. Nat Nanotechnol. 2022; 17: 98-106.
13. Baldwin JG, Heuser-Loy C, Saha T, Schelker RC, Slavkovic-Lukic D, Strieder N, et al. Intercellular nanotube-mediated mitochondrial transfer enhances T cell metabolic fitness and antitumor efficacy. Cell. 2024; 187: 6614-30.e21.
14. Wang Y, Liu X, Huang W, Liang J, Chen Y. The intricate interplay between HIFs, ROS, and the ubiquitin system in the tumor hypoxic microenvironment. Pharmacol Ther. 2022; 240: 108303.
15. Wang M, Zhao X, Zhu D, Liu T, Liang X, Liu F, et al. HIF-1α promoted vasculogenic mimicry formation in hepatocellular carcinoma through LOXL2 up-regulation in hypoxic tumor microenvironment. J Exp Clin Cancer Res. 2017; 36: 60.
16. Zhao Q, Zhu Z, Xiao W, Zong G, Wang C, Jiang W, et al. Hypoxia-induced circRNF13 promotes the progression and glycolysis of pancreatic cancer. Exp Mol Med. 2022; 54: 1940-54.
17. Liu X, Liu L, Chen K, Sun L, Li W, Zhang S. Huaier shows anti-cancer activities by inhibition of cell growth, migration and energy metabolism in lung cancer through PI3K/AKT/HIF-1α pathway. J Cell Mol Med. 2021; 25: 2228-37.
18. Shan T, Chen S, Chen X, Wu T, Yang Y, Li S, et al. M2-TAM subsets altered by lactic acid promote T-cell apoptosis through the PD-L1/PD-1 pathway. Oncol Rep. 2020; 44: 1885-94.

19. Huang X, Zhou W, Zhang Y. Transcription factor YY1 enhances the stemness of lung cancer cells by stabilizing hypoxia factor HIF-1α under a hypoxic microenvironment. Environ Toxicol. 2021; 36: 114-22.
20. Jiang Z, Zhang C, Liu X, Ma X, Bian X, Xiao X, et al. Dexamethasone inhibits stemness maintenance and enhances chemosensitivity of hepatocellular carcinoma stem cells by inducing deSUMOylation of HIF-1α and Oct4. Int J Oncol. 2020; 57: 780-90.
21. Sun X, Lv X, Yan Y, Zhao Y, Ma R, He M, et al. Hypoxia-mediated cancer stem cell resistance and targeted therapy. Biomed Pharmacother. 2020; 130: 110623.
22. Ming L, Cheng K, Chen Y, Yang R, Chen D. Enhancement of tumor lethality of ROS in photodynamic therapy. Cancer Med. 2021; 10: 257-68.
23. Shah R, Ibis B, Kashyap M, Boussiotis VA. The role of ROS in tumor infiltrating immune cells and cancer immunotherapy. Metabolism. 2024; 151: 155747.
24. Gregory CD. Hijacking homeostasis: regulation of the tumor microenvironment by apoptosis. Immunol Rev. 2023; 319: 100-27.
25. Liu J, Hong M, Li Y, Chen D, Wu Y, Hu Y. Programmed cell death tunes tumor immunity. Front Immunol. 2022; 13: 847345.
26. Hyun J, Kim SJ, Cho SD, Kim HW. Mechano-modulation of T cells for cancer immunotherapy. Biomaterials. 2023; 297: 122101.
27. Raskov H, Orhan A, Christensen JP, Gögenur I. Cytotoxic $CD8^+$ T cells in cancer and cancer immunotherapy. Br J Cancer. 2021; 124: 359-67.
28. Zhang XC, Wang J, Shao GG, Wang Q, Qu X, Wang B, et al. Comprehensive genomic and immunological characterization of Chinese non-small cell lung cancer patients. Nat Commun. 2019; 10: 1772.
29. Zhao C, Qiao C, Zong L, Chen Y. Long non-coding RNA-CCAT2 promotes the occurrence of non-small cell lung cancer by regulating the Wnt/β-catenin signaling pathway. Oncol Lett. 2018; 16: 4600-6.
30. Lim ZF, Ma PC. Emerging insights of tumor heterogeneity and drug resistance mechanisms in lung cancer targeted therapy. J Hematol Oncol. 2019; 12: 134.
31. Sun Y, Shen W, Hu S, Lyu Q, Wang Q, Wei T, et al. METTL3 promotes chemoresistance in small cell lung cancer by inducing mitophagy. J Exp Clin Cancer Res. 2023; 42: 65.
32. Terlizzi M, Colarusso C, Pinto A, Sorrentino R. Drug resistance in non-small cell lung Cancer (NSCLC): impact of genetic and non-genetic alterations on therapeutic regimen and responsiveness. Pharmacol Ther. 2019; 202: 140-8.
33. Zugazagoitia J, Paz-Ares L. Extensive-stage small-cell lung cancer: first-line and second-line treatment options. J Clin Oncol. 2022; 40: 671-80.
34. Bamji-Stocke S, van Berkel V, Miller DM, Frieboes HB. A review of metabolism-associated biomarkers in lung cancer diagnosis and treatment. Metabolomics. 2018; 14: 81.
35. Cryer AM, Thorley AJ. Nanotechnology in the diagnosis and treatment of lung cancer. Pharmacol Ther. 2019; 198: 189-205.
36. Pan F, Feng L, Liu B, Hu Y, Wang Q. Application of radiomics in diagnosis and treatment of lung cancer. Front Pharmacol. 2023; 14: 1295511.
37. Xu K, Zhang C, Du T, Gabriel ANA, Wang X, Li X, et al. Progress of exosomes in the diagnosis and treatment of lung cancer. Biomed Pharmacother. 2021; 134: 111111.
38. Vasan K, Werner M, Chandel NS. Mitochondrial metabolism as a target for cancer therapy. Cell Metab. 2020; 32: 341-52.
39. Zong Y, Li H, Liao P, Chen L, Pan Y, Zheng Y, et al. Mitochondrial dysfunction: mechanisms and advances in therapy. Signal Transduct Target Ther. 2024; 9: 124.
40. Guerra F, Arbini AA, Moro L. Mitochondria and cancer chemoresistance. Biochim Biophys Acta Bioenerg. 2017; 1858: 686-99.
41. Shin S, Kwon YJ, Ye DJ, Baek HS, Kwon TU, Kim D, et al. Human steroid sulfatase enhances aerobic glycolysis through induction of HIF1α and glycolytic enzymes. Biochim Biophys Acta Mol Basis Dis. 2019; 1865: 2464-74.
42. Apel K, Hirt H. Reactive oxygen species: metabolism, oxidative stress, and signal transduction. Annu Rev Plant Biol. 2004; 55: 373-99.
43. Bazhin AV, Philippov PP, Karakhanova S. Reactive oxygen species in cancer biology and anticancer therapy. Oxid Med Cell Longev. 2016; 2016: 4197815.
44. Zhang J, Wang X, Vikash V, Ye Q, Wu D, Liu Y, et al. ROS and ROS-mediated cellular signaling. Oxid Med Cell Longev. 2016; 2016: 4350965.
45. Zhang J, Duan D, Song ZL, Liu T, Hou Y, Fang J. Small molecules regulating reactive oxygen species homeostasis for cancer therapy. Med Res Rev. 2021; 41: 342-94.
46. Lennicke C, Cochemé HM. Redox metabolism: ROS as specific molecular regulators of cell signaling and function. Mol Cell. 2021; 81: 3691-707.
47. Movahed ZG, Yarani R, Mohammadi P, Mansouri K. Sustained oxidative stress instigates differentiation of cancer stem cells into tumor endothelial cells: pentose phosphate pathway, reactive oxygen species and autophagy crosstalk. Biomed Pharmacother. 2021; 139: 111643.
48. Tuy K, Rickenbacker L, Hjelmeland AB. Reactive oxygen species produced by altered tumor metabolism impacts cancer stem cell maintenance. Redox Biol. 2021; 44: 101953.
49. Ribas A. T cells as the future of cancer therapy. Cancer Discov. 2021; 11: 798-800.
50. Wei J, Zheng W, Chapman NM, Geiger TL, Chi H. T cell metabolism in homeostasis and cancer immunity. Curr Opin Biotechnol. 2021; 68: 240-50.

Cite this article as: Lin S, Yuan L, Chen X, Chen S, Wei M, Hao B, et al. Mitochondrial transplantation sensitizes chemotherapy to inhibit tumor development by enhancing anti-tumor immunity. Cancer Biol Med. 2025; 22: 648-671. doi: 10.20892/j.issn.2095-3941.2024.0596